

Claremont Colleges

Scholarship @ Claremont

CGU Theses & Dissertations

CGU Student Scholarship

Fall 2019

Oscillatory Flow Driven by Cavity

Jeremy Ralph Bonifacio
Claremont Graduate University

Follow this and additional works at: https://scholarship.claremont.edu/cgu_etd



Part of the [Aerodynamics and Fluid Mechanics Commons](#)

Recommended Citation

Bonifacio, Jeremy Ralph. (2019). *Oscillatory Flow Driven by Cavity*. CGU Theses & Dissertations, 365. https://scholarship.claremont.edu/cgu_etd/365.

This Open Access Dissertation is brought to you for free and open access by the CGU Student Scholarship at Scholarship @ Claremont. It has been accepted for inclusion in CGU Theses & Dissertations by an authorized administrator of Scholarship @ Claremont. For more information, please contact scholarship@cuc.claremont.edu.

Oscillatory Flow Driven by Cavity

by

Jeremy Ralph Bonifacio

Claremont Graduate University and California State University Long Beach

2019

Approval of the Dissertation Committee

This dissertation has been duly read, reviewed and critiques by the Committee listed below, which hereby approves the manuscript of Jeremy Ralph Bonifacio as fulfilling the scope and quality requirements for meriting the degree of PhD in Engineering and Applied Industrial Mathematics.

Hamid Rahai, Chair
California State University Long Beach
College of Engineering Associate Dean for Research and Graduate Studies

Marina Chugunova
Claremont Graduate University
Mathematics
Associate Professor

Roger Lo
California State University Long Beach
Chemical Engineering
Associate Professor

Ali Nadim,
Claremont Graduate University
Mathematics
Professor

Abstract

Oscillatory Flow Driven by Cavity

By

Jeremy Ralph Bonifacio

Claremont Graduate University: 2019

Flows past a cavity are known to exhibit an oscillatory behavior with an amplitude and frequency dependent on the incoming flow properties and the geometry of the cavity. Experiments and numerical analyses have been performed to determine the effects of a flow passing through an axisymmetric cavity and discharging into a transverse freestream. The study focuses on the mechanisms involved in the generation of pulsatile flow and its influences on a jet in crossflow. Flow characteristics through the cavity and the jet in crossflow interaction were analyzed using the computational fluid dynamics software Siemens Star-CCM+. The experimental analysis utilized a Laser Doppler Velocimetry (LDV) system for measurements of velocity profiles to determine the oscillatory jet flow properties as well as the oscillation frequency. Cavity dimensions with a Length to Depth ratio of 2 was used with an incoming flow mean velocity of 50 m/s resulting in a turbulent jet with a Reynolds number of approximately 33,600. The flow through the cavity emitted an oscillatory flow at 66.68 Hz determined by a Power Spectral Density plot. The oscillatory flow in cross flow exhibited a lower jet trajectory when compared to a steady jet in crossflow and indicates increased vorticity production within the jet, supporting flow recovery immediately downstream of the jet. The passive approach of generating an oscillatory jet in crossflow can aid in mixing of the two flows. Also included in the study is an application of the cavity driven oscillatory flow as it pertains to the upper respiratory system.

Dedication

To my loving wife Phileya

Acknowledgements

I would like to express my gratitude to all those who helped me complete this Dissertation. I want to thank Dr. Hamid Rahai for his support and guidance throughout the research and writing process of this Dissertation. I would like to thank my dissertation committee members Dr. Roger Lo (CSULB), Dr. Marina Chugunova (CGU) and Dr. Ali Nadim (CGU) for taking the time to review my dissertation. I want to thank Dr. Shahab Taherian, Komal Gada, Ryan Moffat, Leo Torres and Emily Ngo for their technical assistance in the numerical and experimental analyses. I also want to thank my parents Arturo and Cherry Bonifacio and the rest of my family for all their love and support which lead to the fulfillment of my degree.

Table of Contents

Dedication	iv
Acknowledgements.....	v
List of Figures	vii
Chapter 1.....	1
Introduction	1
Chapter 2.....	2
Background	2
Open Cavity.....	2
Acoustic Research	6
Flow into Expansion	6
Jet driven Oscillations	6
Symmetric and Axisymmetric cavities	8
Jet in Crossflow	10
Chapter 3.....	13
Part 1 - Numerical Analysis	13
Numerical Setup.....	13
Results & Discussion	18
Part 2 - Experimental	32
Experimental Setup.....	32
Results & Discussions	34
Chapter IV	43
Effects of Oscillatory flow on the Human Respiratory System	43
Objective	43
Background	43
Numerical Analysis.....	47
Results & Discussions	49
Chapter V	54
Conclusions	54
References	55

List of Figures

Figure 1: Sketch of an Open Cavity. Reprinted from Internaitonal Journal of heat and Fluid Flow, Vol. 32, Seena, A., Sung, H., Dynamic Mode Decomposition of Turblent Cavity Flows for Self-Sustained Oacillations, P. 1098-1110, 2011, with permission from Elsevier	2
Figure 2: Flow in an Open Cavity (Faure 2007). Reprinted from Experiments in fluids by MERZKIRCH, W Reproduced with permission of SPRINGER-VERLAG in the format Thesis/Dissertation via Copyright Clearance Center	3
Figure 3: Double cavity configuration (Tuerke 2017). Experiments in fluids by MERZKIRCH, W Reproduced with permission of SPRINGER-VERLAG in the format Thesis/Dissertation via Copyright Clearance Center.	9
Figure 4: Jet in Cross Flow Reptinted from Fric, T., Roshko, A., Vortical Structure in the Wake of a Transverse Jet, The Journal of Fluid Mechanics, Vol. 279, P. 1-47, reproduced with permission.....	11
Figure 5: Pipe-jet with cavity and the computational domain.	15
Figure 6: Numerical model of (a) Pipe jet (b) Jet with annular duct and (c) Jet origin and coordinate system.	16
Figure 7: Grid distribution: (a) Domain, (b) Mid-section view of the domain, (c) close mid-section view of the jet cavity, and (d) cross-section view of the jet.	17
Figure 8: Axial contours (a) mean velocity, (b) vorticity, and (c) particles velocity for the pipe-jet in crossflow.	19
Figure 9: Spanwise contours of the (a) mean velocity, (b)pressure, (c) vorticity, and (d) velocity vector at $x/d=1$ for the pipe-jet in crossflow.....	20
Figure 10: Contours of the axial mean velocity at the mid-section plane for pipe-jet.	21
Figure 11: Axial contours of (a) mean velocity, (b) vorticity and (c) particle velocity for the pipe-jet with cavity.....	22

Figure 12: Spanwise contours of the (a) mean velocity, (b) pressure, (c) vorticity, and (d) velocity vector at $x/d=1$ for the pipe-jet with cavity in crossflow.	23
Figure 13: Contours of the (a) mean velocity and (b) vorticity, and (c) velocity vector within the cavity.	24
Figure 14: Axial mean velocity profiles along the mid-section plane.	26
Figure 15: Spanwise vorticity contours	28
Figure 16: Jet trajectory, (a) Pipe jet, (b) Pipe Jet with cavity	31
Table 1: Power coefficients.	31
Figure 17: Experimental setup	32
Figure 18: Axial mean velocity of Pipe Jet Experiments.....	34
Figure 19: Axial mean velocity profiles of Jet with Cavity Experiments.....	35
Figure 20: Axial Turbulence Intensity for a Pipe Jet.....	36
Figure 21: Axial Turbulence Intensity of a Pipe-jet with Cavity.....	37
Figure 22: Experimental Trajectory plots of (a) Pipe jet and (b) Pipe Jet with cavity.....	38
Table 2. Experimental Power coefficients.	38
Figure 23: Flow of a Pipe Jet (left) and Pipe Jet with Cavity(right).....	39
Figure 24: Power Spectral Densities for Pipe Jet in (a) Linear Scale and (b) Log-Log Scale.....	40
Figure 25: Power Spectral Densities for Pipe-Jet with Cavity in (a) Linear Scale and (b) Log-Log Scale.....	41
Table 3: Variation of Strouhal Number with Reynolds Number.....	42
Figure 26: Respiratory System.....	44
Figure 27: Inhalation and Oscillation Velocity Curve.....	46
Figure 28: 3D Trachea Model.....	47
Figure 29: Percentage Deposition Change of Mixed Flow Comparison for the Left and Right Lobe.....	50
Figure 30: Percentage Comparison for Particle and Velocity Oscillation Matching Frequencies for the Left and Right Lobe.....	52
Figure 31: Comparison of Amplitude Change for both Left and Right Lobe.....	53

Chapter 1

Introduction

Cavity driven flows are flows that can create oscillations due to i) the jet instability as it enters the surrounding fluid and ii) the shear driven portion that generates a primary vorticity inside the cavity. Research in cavity driven flows have applications in Aerospace, Civil, and Biomedical Engineering, among others. Flow buffeting occurs from opening of a landing gear door, a bomb door, or even an open cockpit. Sediment deposition in rivers and flow in larynx are other examples of cavity flows. Cavity flows can create oscillations (Rossiter 1964), generate noise, increase drag (Gharib and Roshko, 1987) and develop instabilities in aircraft operation.

To better understand how the oscillatory flow is made through a cavity, studies are broken down to smaller fundamental studies analyzing the flow passing through an expansion section, a jet instability in a confined cavity and how the shear layer interactions with the edge of the cavity creates oscillations.

Areas of interest that the cavity oscillatory flow can alter the mixing characteristic is the application of an oscillatory jet in cross flow. Vermeulen (1990) analyzed a pulsatile flow in cross flow with a speaker device attached parallel to the jet inlet. In the majority of the studies active controllers were used in generating oscillatory jets. The use of a passive controller for the jet oscillation can minimize the complexity of creating a pulsatile jet. In the present study, numerical and experimental investigations of a cavity driven oscillatory flow discharging perpendicularly into a crossflow have been investigated and results were compared with corresponding results of a steady jet in cross flow. As the results will show, the flow interactions of the cavity driven oscillatory jet in crossflow have increased mixing as compared to of mixing of a steady jet in cross flow. In the last chapter, results of an investigation into using the oscillatory cavity driven flow for controlling particles (aerosols) deposition in the human upper respiratory system are presented.

Chapter 2

Background

Open Cavity

Figure 1 and 2 illustrate an open cavity and its flow characteristics. The incoming boundary layer, either laminar or turbulent, enters the cavity and interacts with the shear layer. Slight oscillation generated in the separated shear layers results in impingement of the shear layer on the downstream top corner of the cavity, resulting in flow a clockwise recirculation inside the cavity that could extend to near the front wall. A counter-clockwise recirculation is also formed near the front wall. These two vortices impinging on the shear layers, for increased oscillation. The mechanism repeats itself for a sustained oscillation. Charwat (1961) defines the open cavity flow as the incoming flow attached to the upwind horizontal wall, passes through the cavity section and as the flow approaches the far wall, the flow then reattaches to the downstream wall. A shallow cavity is where the length of the channel to its depth is greater than 1 and a deep channel is where the ratio is less than 1 (Sarohia 1977). Flows over the cavity can be either incompressible or compressible depending on the flow velocity or Mach number.

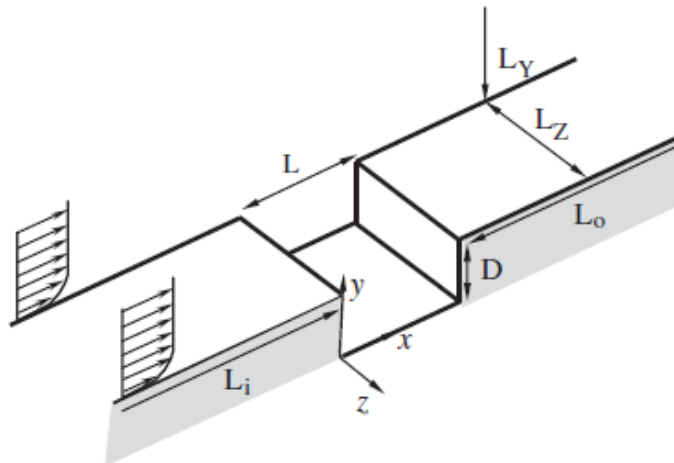


Figure 1: Sketch of an Open Cavity. Reprinted from *International Journal of heat and Fluid Flow*, Vol. 32, Seena, A., Sung, H., *Dynamic Mode Decomposition of Turblent Cavity Flows for Self-Sustained Oacillations*, P. 1098-1110, 2011, with permission from Elsevier

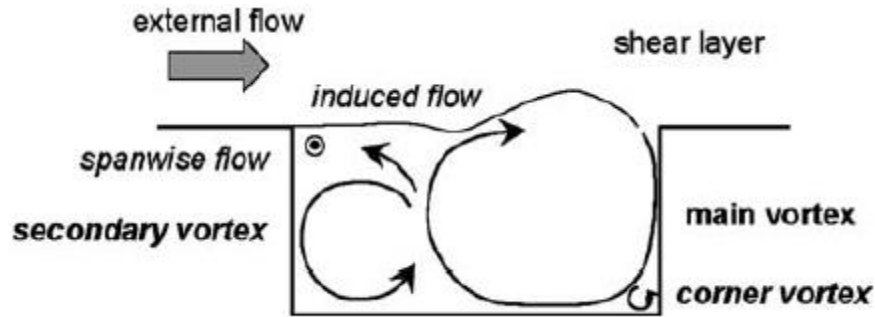


Figure 2: Flow in an Open Cavity (Faure 2007). Reprinted from *Experiments in fluids* by MERZKIRCH, W. Reproduced with permission of SPRINGER-VERLAG in the format Thesis/Dissertation via Copyright Clearance Center

Rockwell (1979) investigated both the unstable flow past a cavity and the vortex edge interaction as a driving mechanism in the cavity. Using Hydrogen bubbles visualization techniques, and LDV measurements, he first analyzed the edge interaction of the flow hitting the top downstream corner of the cavity and determined the rolling frequencies of the edge vorticity. He then analyzed the 3-D nature of the unstable flow inside the cavity. The large recirculating flow inside the cavity are generated by the shear layer of the flow over the cavity and the edge interaction of the back wall creates a three dimensional flow inside the cavity. Wang's (2015) numerical results using LES confirmed this driving mechanism.

Neary (1987) identified three regions of flow over an open cavity: a) Regime 1 - is characterized by pressure oscillations in the cavity that vary slightly with time, b) Regime 2 – has an intermittency pressure time trace and two non-proportional frequencies what are further apart than regime 1, and c) Regime 3 – where the pressure oscillations vary strongly with time. He concluded that for each regime, there were strong shear-layer oscillations and the oscillations were stronger near the downstream corner of the cavity exit which resulted in larger oscillation amplitudes.

Open cavity investigations of the incoming boundary layer and how it affects the cavity flow were performed experimentally by Grace (2004). She used hot wire anemometry technique and two component LDV and determined with incoming laminar boundary layer, vorticity is 31% stronger than having an upstream turbulent boundary layer. In the turbulent cavity flows of low Mach numbers, four

narrow band frequencies were identified to be between 50 and 500 Hz (Chantellier 2004). This was discovered experimentally using Pressure and PIV measurements. Ozsoy (2005) confirmed from laminar flow conditions in a shallow cavity with different Reynolds numbers that with increasing Reynolds number, the flow entering the cavity exhibits a more jet like behavior. Haigermoser (2008) further investigated the boundary layer influence on cavity flow and identified the length to momentum thickness ratio (L/Θ) greater than 80 will produce a self-sustained oscillation. Here L is the length of the cavity and Θ is momentum thickness of incoming boundary layer.

Ashcroft (2005), Ukeiley (2005), and Faure (2006) experimentally investigated the effects of adjusting the length to depth ratio (L/D) of the cavity. Basley (2013) identified features common to impinging shear flows: a) Kelvin- Helmholtz waves are excited in the shear layer, b) They influence the two cavity edge, which are responsible for an instantaneous feedback-loop based on pressure causing the flow to be unstable and c) Depending on L/θ , one or more frequencies are selected and enhanced.

The investigation to determine mode frequencies for the oscillatory flow in a cavity has been performed experimentally by Lusseryan (2008) and Basley (2011) and numerically by Gloerfelt (2003), Seena (2011), Farkas (2012) and Wang (2015). Lusseryan used LDV measurements at the back edge of the cavity to find the power spectral densities of x-component velocity which revealed two peak frequencies of 23.2 Hz and 31.0 Hz for an open cavity of $L/D = 2$ and Reynolds number of 14,000. The two modes were investigated through phase plots, Poincare sections and return maps which was used to identify mode switches. Basley (2011) investigated the modal frequencies using time resolved PIV and LDV measurements. He determined that the oscillation exhibited a primary frequency with two or three harmonic frequencies. Through direct numerical simulation (DNS), Gloerfelt (2003) identified the two mode switching inside the cavity: Mode I) The shear layer is formed by only one coherent vortex and Mode II) Two individual vortices are seen where one is in the shear layer and one at the downwind edge which were Kelvin-Helmholtz vortices in the shear layer. LES analysis along with Dynamic Mode Decomposition (DMD) of a thick incoming boundary layer into a cavity indicate that the boundary layer

structures and the cavity shear layer structures coincide in both frequency and wave number space (Seena 2011).

So far most of the studies mentioned for the open cavity were related to incompressible flows, however compressible flow with cavity has also been extensively investigated. The experimental investigations of incoming flows with Mach 0.3 to 0.99 by Kegerise (2004), Malone (2009), Murray (2009) and Martinez (2012) and flows of Mach greater than 1 by Kumar (2018) are examples of such investigations. Kegerise (2004), Malone (2009), and Murray (2009) examined the switching of Rossiter modes and their harmonics. Malone (2009) indicated that Rossiter modes will vary with Mach number. Martinez (2012) attempted to control cavity oscillations with placing a cylindrical rod upstream of the cavity. He observed the von Karmen vortices shedding into the flow from the cylinder decays rapidly in the cavity shear layer resulting in the flow not exhibiting the self-sustained oscillation. Kumar (2018) was interested in the effects of the shockwaves produced by the cavity. Numerical investigations were performed by Rowley (2002), Larcheveque (2003), Bres (2008), Yokoyama (2009) and Nair (2017). These studies were focused on 2-D generated self-sustained oscillations and identifying both the mode and mode switching of the flow. Dynamic control reviewed by Rowley (2006) and Cattafesta (2008) and also investigated by Illingsworth (2012) who generated a simple linear model to provide a feedback control of the cavity flow oscillations.

The choice to study a plane jet open flow over an open rectangular cavity was to simplify the problem by focusing on physical characteristics of two dimensional cavity flow. However, since the flow over the cavity are not sufficiently wide, and with secondary flows in the cavity, the flow is three dimensional. Basley (2013) correlates 2 dimensional time resolved data to understand the 3 dimensional flow of the cavity. Guenait (2013) also investigated experimentally the three dimensional flow using DMD and Proper Orthogonal Decomposition to correlate the 2-D flow to 3-D. De Vincente (2014) used both numerical and experimental techniques to understand the evolution of centrifugal instabilities in an open cavity from onset to a saturation state. He identified three main modes of instability in cavity flow with Mode II being the dominant mode as Reynolds number increases.

Acoustic Research

Krisnamurty (1955) studied the acoustic radiation of a flow over a rectangular cavity. He used a schlieren system and hot wire measurements to examine flow through the cavity. The flow was considered to be compressible with Mach number ranged 0.45 to 0.8. At Mach 0.8 a high frequency radiation that was strong and directional were generated from small cavities of 0.1 inch to 0.2 inch wide and 0.1 inch deep. Powell (1961) investigated the edge tones produces as the flow was bifurcated due to a corner. Rossiter (1964) and East (1966) also analyzed experimentally the acoustic effects in flows over a rectangular cavity. However, Rossiter (1964) is credited for identifying the mechanism that generates flow oscillations and is currently coined the “Rossiter Mechanism.” East (1966) analyzed the flows at low Mach numbers over a deep cavity and Tam (1976) then followed the investigations with a numerical analysis to identify acoustic modes of a rectangular cavity.

Flow into Expansion

Flow instabilities in an expansion section was analyzed by Cherdran (1978). He used flow visualization and Laser Doppler Velocimetry (LDV) to study a plane jet encountering a sudden expansion at low Reynolds numbers. It was determined that increasing Reynolds number increases the oscillation frequency emitted by the jet flow. Schreck (2000) used an incompressible Reynolds–Averaged Navier Stokes (RANS) model to study flow bifurcation in a sudden expansion of a 3-D Plane jet and identified critical Reynolds numbers bifurcation points for different aspect ratio’s. For lower aspect ratios, the flow is stabilized and the bifurcation point moves to a higher Reynolds number.

Jet driven Oscillations

Jet flow over a cavity has been investigated to determine the jet instabilities. Results have shown that oscillations are weak at low Reynolds numbers and become self-sustained at higher Reynolds numbers. With increasing Reynolds number, the identifiable frequency peaks grow and broaden (Ern

1995). Maurel (1996) performed experiments using Laser Induced Fluorescence (LIF) techniques. A plane jet was discharged into a cavity and the outlet of a larger opening was in line with the jet flow. For low Reynolds numbers, he established an upper and lower limit wavelength selection criterion. With different Cavity length to diameter ratios and corresponding Reynolds numbers, one can identify if the flow is stable, the flow oscillates due to the free jet, or the flow oscillates from the vorticity interactions generated in the cavity. Kolsek (2016) numerically identified the cavity flow characteristics using a finite volume method. He observed at the large time-scale, such as altering asymmetry jet flow behavior followed by a variety of oscillations of different time and length subscale.

Mataoui (2001, 2008) performed numerical and experimental investigations of a plane jet flowing into a rectangular cavity with the outlet of the cavity on the same side of the jet nozzle. The plane jet was analyzed using hot wire anemometry to collect velocity profiles and he used Unsteady RANS (URANS) for his computational analyses. He identified three zones for the jet over the cavity as: no oscillation, unstable oscillation and stable oscillation as it impinges on the cavity wall. It was concluded that the jet instability is created by the deflection of the jet by the Coanda effect, where fluctuations are produced due to periodic pressure changes along the cavity. The Coanda effect was also investigated by Gloefelt (2008) numerically using LES.

Righolt (2015) numerically analyzed the dynamics of a square jet discharging into a confined cavity where the exit of the cavity was on the far wall but closer to the top wall. The jet exit was not in line with cavity exit. Using Particle Image Velocimetry (PIV) and LES, a zero dimensional numerical model was developed for describing the three phases in self-sustained oscillations as: 1) the pressure driven growth, 2) amplitude limitation by geometry and 3) the delayed destruction of the recirculation zone. A critical Reynolds number formula was also derived to determine the point of stability and instability.

Water jet flow into a cavity was investigated experimentally by Kalter (2013), and numerically by Bensider (2016). Experimental investigations of a submerged bifurcating nozzle in water using PIV

determined that if the depth was large enough then long term self-sustained asymmetric oscillations were produced (Kalter,2013). Bensider (2016) analyzed the effects of a jet flow in a cavity with two opposing jets perpendicular to the main jet. Wenchuan (2017) used both numerical and experimental techniques to determine the effect of a 120 degree impinging edge Helmholtz oscillatory nozzle. They determined that URANS was not the proper choice for the analysis since there was not a sufficient turbulence model to accurately predict the flow.

Neubauer (2007) and Chasari (2011) used a simplified jet into cavity to correlate the flow characteristics of a ridged larynx. Neubauer (2007) used PIV to determine that the flapping of the jet was due to asymmetric vortices the jet produced. Chisari (2011) used Schlieren techniques as well as numerical investigations to analyze the flow through a cavity. He identified the vortex dipole structures as it starts formation in the cavity and from the simplified version of laryngeal flow may lead to the onset of vocal production. However, since the assumption of the larynx is static and of a simplified shape the results may not be transposable to real voice generation mechanism.

Symmetric and Axisymmetric cavities

Symmetric cavities are shaped with two open cavities facing each other as seen in Figure 3. Investigations of a double cavity is performed experimentally by Tuerke (2017). He focused specifically on the double cavity flow and the oscillatory effect they have when the cavities oppose each other. The study was similar to Maurel (1996) however, the inlet pipe height and width were the same dimensions while Maurel (1996) has a smaller inlet height than the exit. Tuerke (2017) shows how the shear layer spectra are affected when the Reynolds number and the distance between the two cavities are adjusted. He identified a steady, periodic, and bi-periodic regime as the Reynolds number is increased. The cavity to cavity distance affected the onset of the regime. As the cavity distances are increased, at a D/L greater than 0.4 results in a spectral signature was similar to a single cavity.

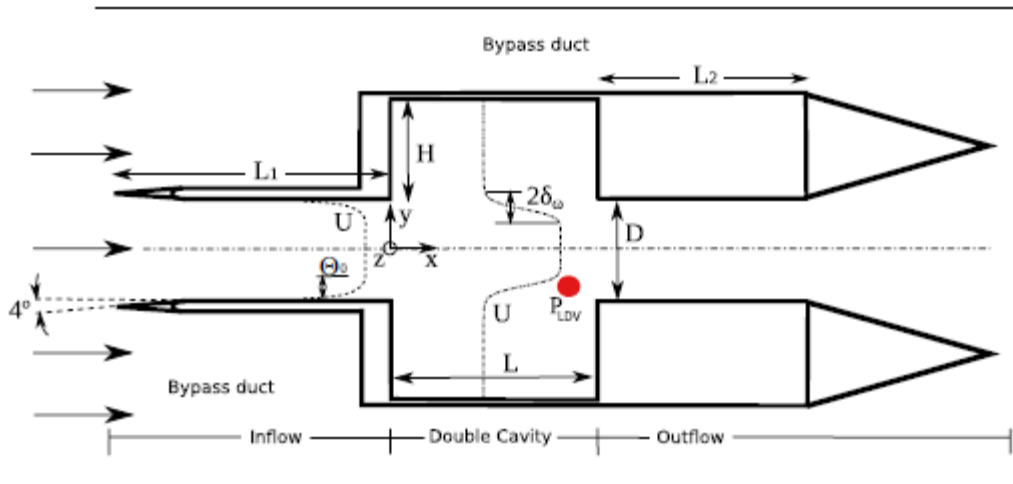


*Figure 3: Double cavity configuration (Tuerke 2017). Experiments in fluids by MERZKIRCH, W
Reproduced with permission of SPRINGER-VERLAG in the format Thesis/Dissertation via Copyright
Clearance Center.*

Axisymmetric shapes can have flow that go over an open cavity (Sarhonia 1977, Gharib 1987,1987) or as in an annular cavity the flow passes through (Rockwell 1979, Shankar 2000). Gharib experimentally identified the oscillation around the leading edge of the cavity through LDV measurements. He also identified above a critical value of cavity length to depth ratio there is an abrupt and large increase in drag due to the wake mode instability which corresponds to changes in cavity pressure. The flow regimes for this study indicated that the flow can be non-oscillating, oscillating and wake mode where the wake mode appears when the cavity length is large. Rockwell (1979) and Shankar (2000) only mention the flow through an annular cavity in their annual review papers, commenting only about its complexity and how two dimensional and three-dimensional annular cavity flow can vary due to the difference of the impinging shear layer on the downstream corner of the cavity. Jet flows into a cavity, flows over an open cavity as well as flows through a double cavity can provide understanding of the characteristics of flow through an annular cavity. The self-sustained oscillation flow characteristics may be similar as the plane jet in cavity investigation of Maurel (1996). Open cavity research simplifies the

possible explanation of how the self-sustained oscillations are created and the characteristics of the feedback mechanism of the cavity vortices.

Jet in Crossflow

Jet in crossflow (JICF) has been studied extensively for its practical applications such as plume dispersion, gas turbine combustor cooling and fuel injection (Ruiz 2015). The technical understanding of optimizing transport and mixing characteristics depends on understanding the mechanics of turbulence and the jet to crossflow interaction. Margason (1993) describes the distinguishable characteristics generated as the jet issues into a cross flow of the free stream. The velocity ratio r is a major factor in shaping the JICF profile as well as determining the jet penetration into the crossflow. Figure 4 shows four identifiable characteristics for the jet in cross flow:

- a) Counter-rotating vortex pair (CVP) is the dominant structure downstream of the jet crossflow interaction. The CVP is generated by the deflection of the jet and is convected downstream by the crossflow. Kelso's (1996) experimental results suggested that the CVP originates in a process of roll-up, tilting and folding of the shear layer vortices. Cortelezzi (2001) has numerically confirmed the CVP formation process.
- b) Horseshoe vortex is caused by adverse pressure gradient just in front of the injection hole. This structure and the vortex-shedding frequency are similar to those of flow around a cylinder (Krothapalli 1990).
- c) Shear-layer ring vortices are generated when the boundary layer of the crossflow and the immediate exit at of the front of the jet interact. These vortices evolve in the flow to help generate the CVP (Kelso 1996, Cortelezzi 2001). These are not present in an elevated jet in cross flow since the jet exit is typically well above the crossflow boundary layer.
- d) Wake vortices are typically seen when $r > 1$. The experiments of Fric & Roshko (1994) suggested that these vortices originate from the wall boundary layer.

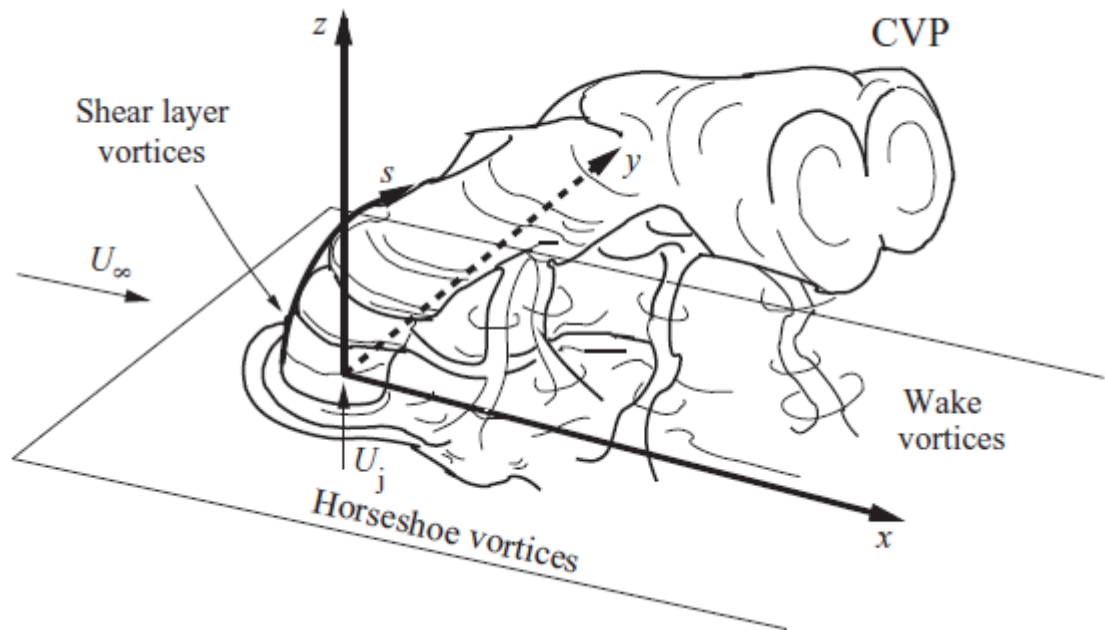


Figure 4: Jet in Cross Flow Reprinted from Fric, T., Roshko, A., Vortical Structure in the Wake of a Transverse Jet, The Journal of Fluid Mechanics, Vol. 279, P. 1-47, reproduced with permission.

Vermeulen (1990), Eroglu (2001), Johari (2006) and Huang (2012) experimentally investigated the pulsed jet in cross flow. Vermeulen (1990) analyzed different velocity ratios, determining that the optimal response for the jet pulse correlates to $St = 0.22$. A strong resonance mode of 208 Hz was identified and used this for the frequency for all velocity ratios. Toroidal vortices shedding at the jet outlet were observed which produced changes in the jet structure. An increase of up to 92% was seen for jet penetration as well and in spreading and mixing rate. Eroglu (2001) analyzed the pulse jet vortex rings and determined that the space and strength was dictated by the pulse of the jet. He saw that the rings generated from the pulse jet interaction formed a distinct vortex look merging pattern that was made up of the curved shear layer around the jet which was confirmed numerically by Sau (2010). Eroglu (2001) concluded with an optimal pulse strength frequency and duty cycle, a 70% increase in jet penetration can be achieved. Coussement (2012) numerically determined that there is a link between the intensity of the vortex emitted with a velocity increase of the pulsed signal proving that the more the velocity increases, the more the vortex emitted will be coherent, independently of the duty cycle. Johari (2006) identified the

penetration of a fully pulsed jet scales with the fourth root of the velocity ratio, stroke and axial distance with a decay of the mean concentration scales with the velocity ratio and axial distance to the negative three – fourths power.

Chapter 3

Part 1 - Numerical Analysis

Numerical Setup

The computational analyses were performed using Siemens Star CCM+ software. Star CCM+ processes calculations using different sets of algorithms that are defined by each model properties to solve various outputs with the given inputs. A URANS approach was selected and the basic calculations that the program uses to provide results are standard fluid flow equations, which are listed in Siemens Star CCM+ user manual.

The program uses the continuity equation,

$$\frac{d}{dt} \int_V \rho dv + \oint_A \rho(v - v_g) \cdot da = 0 \quad (1)$$

along with the momentum equation,

$$\begin{aligned} \frac{d}{dt} \int_V \rho v dV + \oint_A \rho v \times (v - v_g) \cdot da = \\ - \oint_A p I \cdot da + \oint_A T \cdot da + \int_V (f_r + f_g + f_p + f_u) dV, \end{aligned} \quad (2)$$

where T is the complete stress tensor given by,

$$T = T_l + T_t.$$

An incompressible fluid flow using pressure-velocity coupled flow solver was used with hybrid turbulence model combining Wilcox K- ω and the K- ϵ models, known as the K- ω SST turbulence model. The K- ω SST model uses two terms, the K term (turbulent kinetic energy) and the Omega (ω) term (specific dissipation rate $\omega \sim \epsilon / K$) which is approximated as the dissipation rate divided by the Turbulent Kinetic Energy (TKE). Advantage of the Wilcox K- ω over K- ϵ is an improved performance for boundary layers under adverse pressure gradients. Another advantage, as opposed to the K- ϵ turbulence model is it

provides higher accuracy for complex flows conditions (Pope 2000). However, the disadvantage to the K- ω turbulence model is that the boundary layer computations are very sensitive to values in the free stream. This hybrid model uses the K- ω model near the wall, while in freestream the K- ϵ model is used.

The basic transport equations used for K- ω SST are

$$\frac{d}{dt}(\rho k) + \nabla \cdot (\rho k \bar{v}) = \nabla \cdot [(\mu + \sigma_k \mu_t) \nabla k] + G_k + G_{nl} + G_b - \rho \beta^* f_{\beta^*} (\omega k - \omega_0 k_0) + S_k \quad (3)$$

and

$$\frac{d}{dt}(\rho \omega) + \nabla \cdot (\rho \omega \bar{v}) = \nabla \cdot [(\mu + \sigma_\omega \mu_t) \nabla \omega] + G_\omega + D_\omega - \rho \beta f_\beta (\omega^2 - \omega_0) + S_\omega \quad (4)$$

And the turbulence production terms are

$$G_k = \mu_t S^2 - \frac{2}{3} \rho k \nabla \cdot v - \frac{2}{3} \mu_t (\nabla \cdot v)^2 \quad (5)$$

and

$$G_\omega = \rho \gamma \left[\left(S^2 - \frac{2}{3} (\nabla \cdot \bar{v})^2 \right) - \frac{2}{3} \omega \nabla \cdot \bar{v} \right]. \quad (6)$$

The numerical model, based on finite volume method, was constructed using the Solidworks software and was imported into Siemens STAR-CCM+ software. The computational domain extends 2.286 m. x 2.032 m. x 1.27 m. in axial, normal and spanwise directions (x, y and z) respectively. Figure 5 shows the computational domain with inlets and outlet boundary conditions and the pipe-jet with and without cavity.

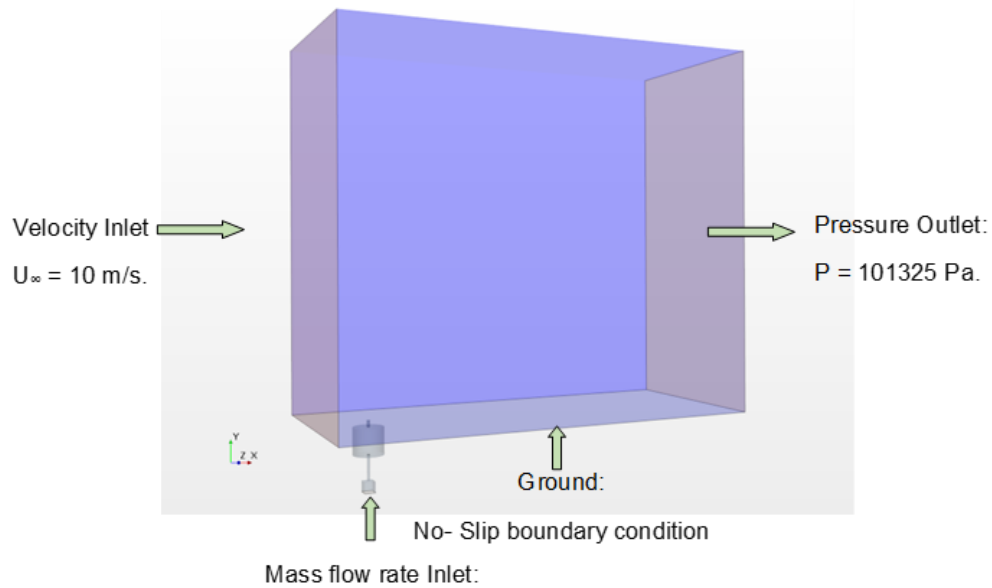


Figure 5: Pipe-jet with cavity and the computational domain.

The pipe-jet diameter, d , was 1.27 cm. It was placed at the bottom plane midsection at $20d$ from the entrance (Fig. 6a). The pipe length was $24d$ with $2d$ protruded from the bottom surface. At the pipe inlet, a cubic plenum with $4d$ in length, width and height was added to provide numerical stability for accurate results. For the jet with cavity (Fig 6b), the cavity length and diameter were $20d$ each. The Reynolds number for the round jet is approximately 33,600 and the cavity Reynolds number of 336,000 for the $r=4$ velocity ratio. The cavity was located at $4.5d$ from the jet exit. For the cavity, the $L/r_c = 2$. Here r_c is the depth of the cavity.

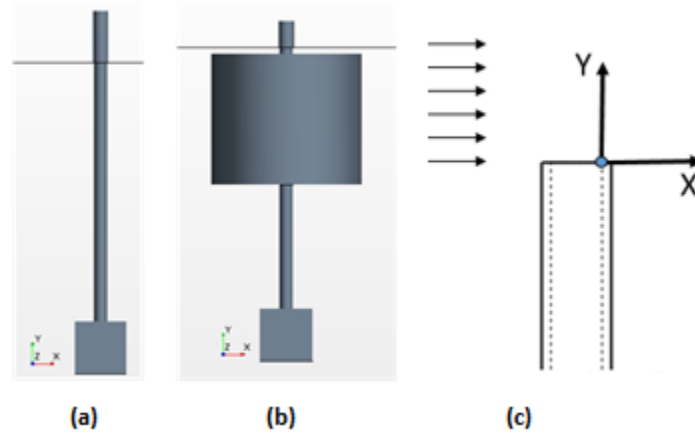


Figure 6: Numerical model of (a) Pipe jet (b) Jet with annular duct and (c) Jet origin and coordinate system.

The computational grid domain as shown in Figure 7 (a) – (d) consists of a hybrid mesh topology with approximately 2.3 million cells for the baseline model and approximately 6.5 million cells for jet with cavity. Mesh independency was performed for both cases with baseline model ranging from approximately 0.3 million cells to 16 million cells and for jet with cavity ranging from approximately 0.5 million cells to 38 million cells. An 18 layer structured hexahedral grid of 2 mm thickness from the wall with a growth rate of 1.3 was constructed with wall y^+ value less than 1 for all the simulations. A refined conical grid region as shown in Figure 7(b) was constructed at the jet outlet in the streamline direction to increase the accuracy of the jet trajectories and flow characteristics. Unstructured polyhedral grid was created away from wall to minimize total number of cells, reducing computational time.

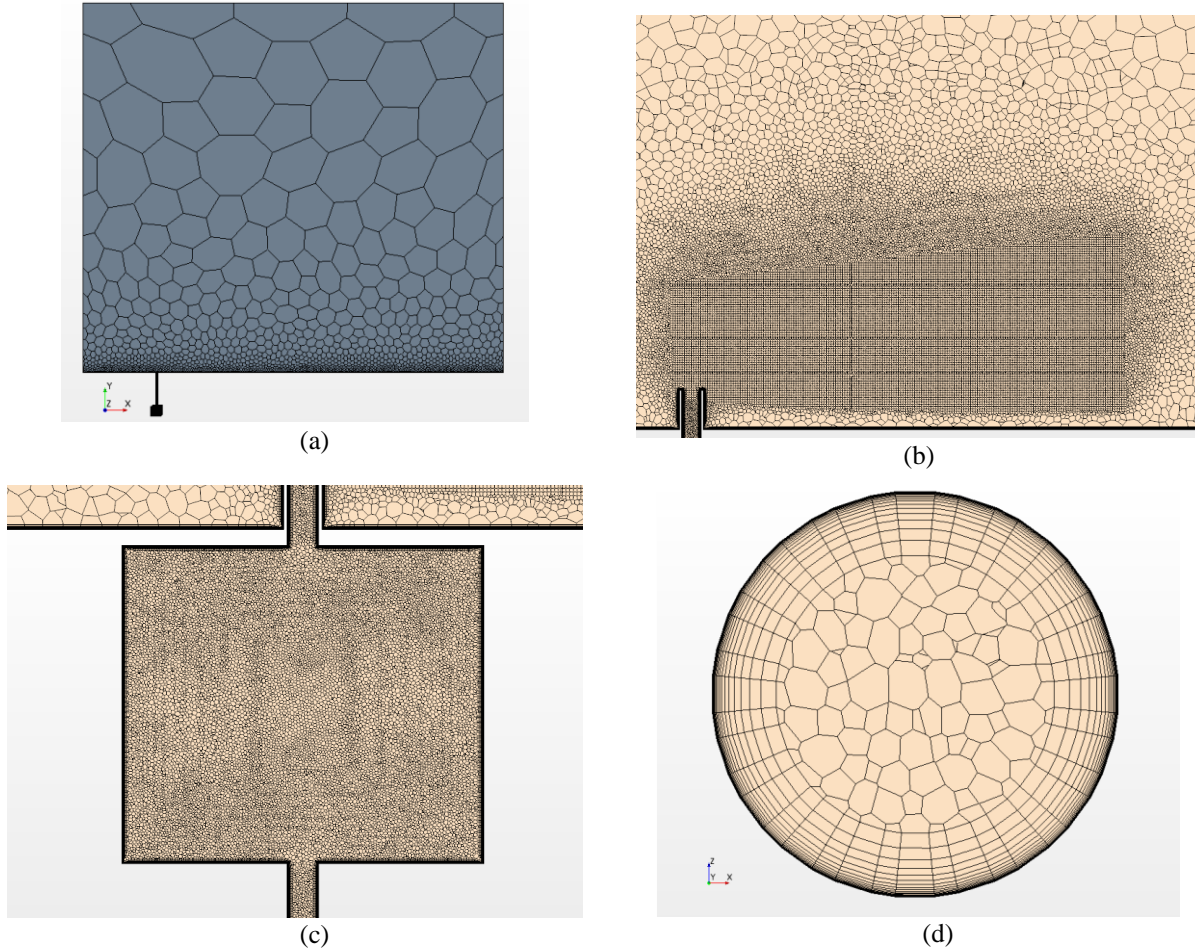


Figure 7: Grid distribution: (a) Domain, (b) Mid-section view of the domain, (c) close mid-section view of the jet cavity, and (d) cross-section view of the jet.

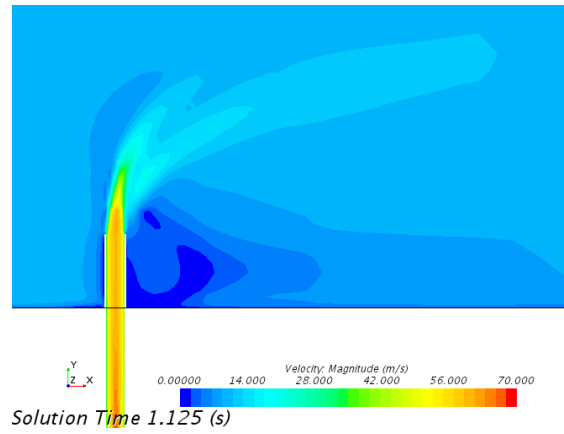
A second order discretization of Implicit time-stepping was performed with a time step of $\Delta t = 0.001$ sec for 1 sec. total duration when particles were not introduced into the flow and 4 sec. with particles in the flow. For an accurate averaging, 10 iterations were performed for each time – step. The particles used were solid carbon with $1 \mu\text{m}$ diameter. They were injected at the Jet inlet plenum as a surface injector with a mass flow rate of $7.76\text{e-}4$ kg/s. All results presented are after the simulations reaching a steady state, i.e. the shedding frequency remains constant. Also we made sure that the residuals for solving the continuity, the momentum, and the turbulent kinetic energy (T.K.E.) equations, and the rate of turbulent dissipation rate were dropped by significant orders of magnitude with no further change in the results under the tolerance value of 10^{-4} . All simulations were performed on a 36 core Xeon desktop. Each run time took an

average of 120 hours and approximately 28,000 – 30,000 iterations, before reaching the steady - state solution.

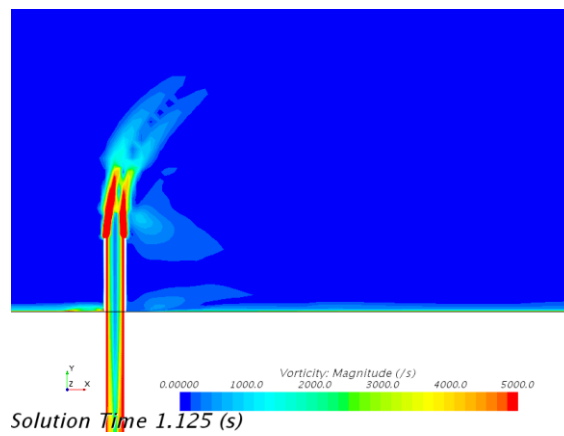
Results & Discussion

Selective contours seen in figures 8 and 9 are in the axial and spanwise directions respectively for the steady pipe-jet in cross flow. The pipe-jet initially penetrated vertically into the cross flow, then tilts into the crossflow direction. Increased vortex interactions are seen between the initial shear layers and the crossflow which reduces downstream. The counter rotating vortices are observed at $x/d = 1$ and shown to have a high pressure on the top with pressure and velocity gradients around the jet column. The particles' velocities are reduced as the jet fully tilts into cross flow following the jet momentum trajectory.

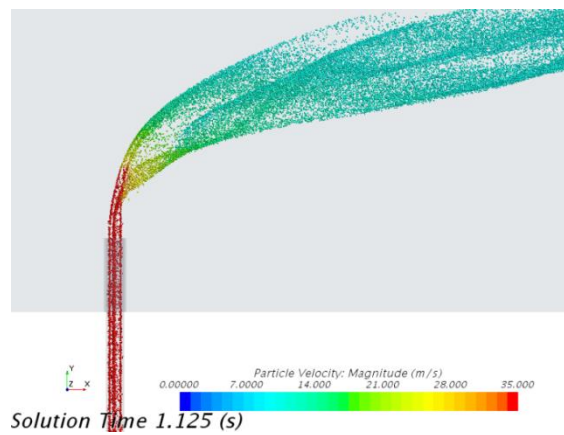
Axial mean velocity contours at the mid-section plane at different locations for the pipe-jet are presented in figure 10. The $x/d = 0$ profile is similar to a distorted top-hat profile which becomes more pronounced at $x/d=1$. Immediately downstream, the two peak velocity points are reduced to one and the profile shows similar characteristics of a jet in cross flow with the maximum velocity elevated with downstream distance.



(a)

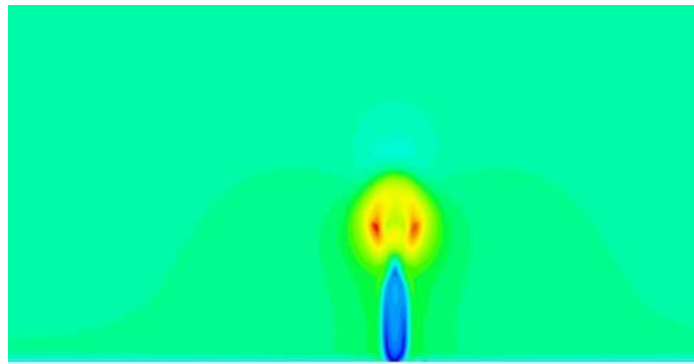


(b)

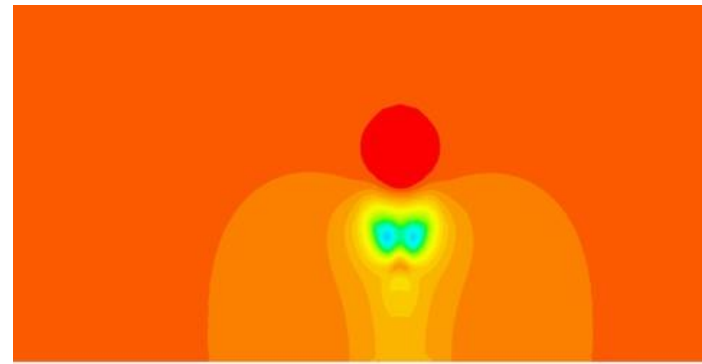


(c)

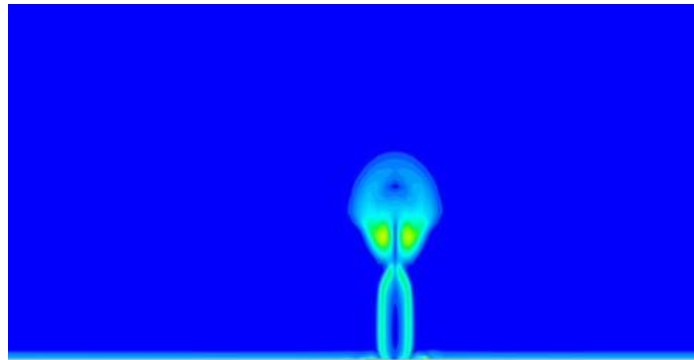
Figure 8: Axial contours (a) mean velocity, (b) vorticity, and (c) particles velocity for the pipe-jet in crossflow.



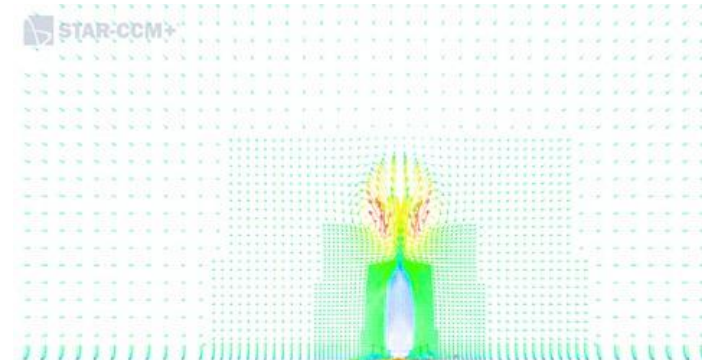
(a)



(b)



(c)



(d)

Figure 9: Spanwise contours of the (a) mean velocity, (b) pressure, (c) vorticity, and (d) velocity vector at $x/d=1$ for the pipe-jet in crossflow.

Velocity Profiles

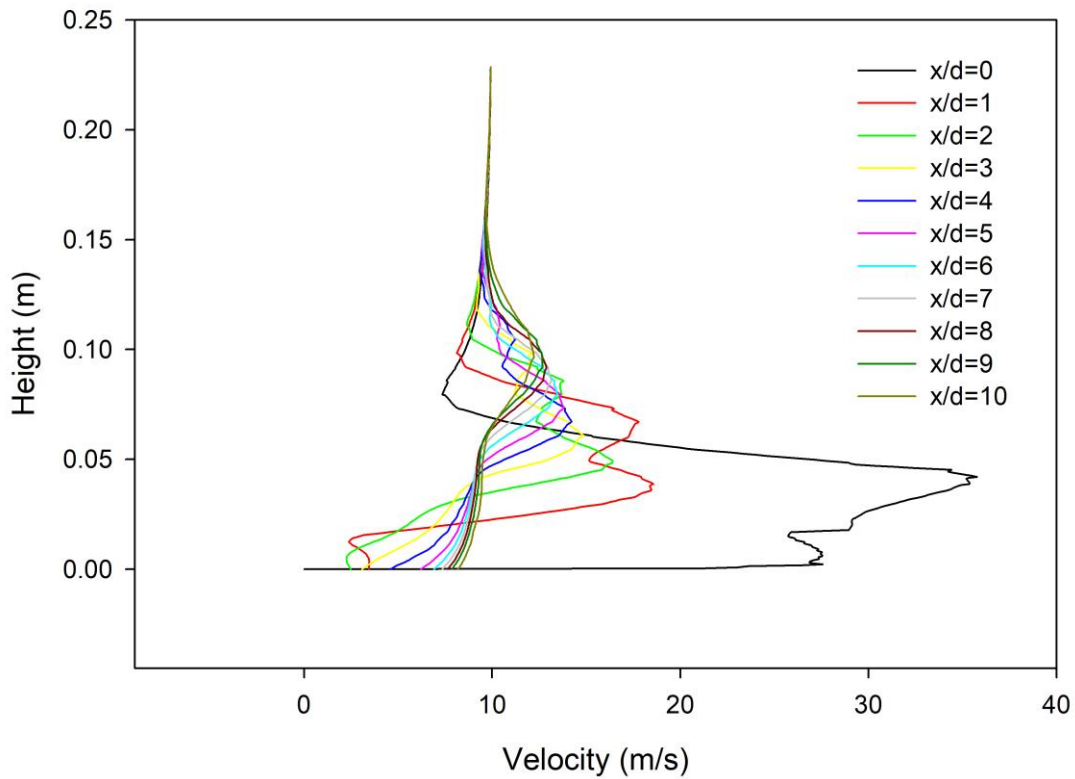
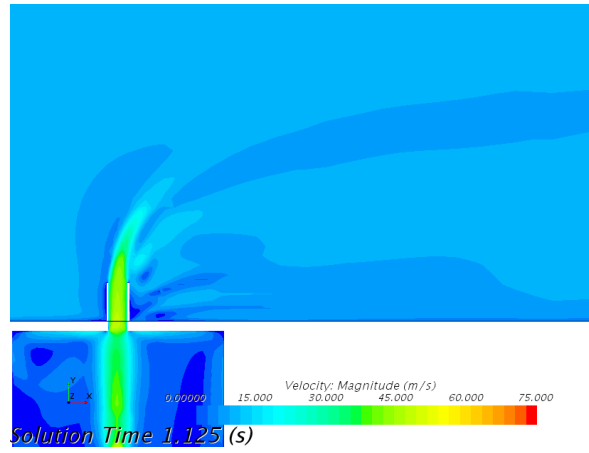
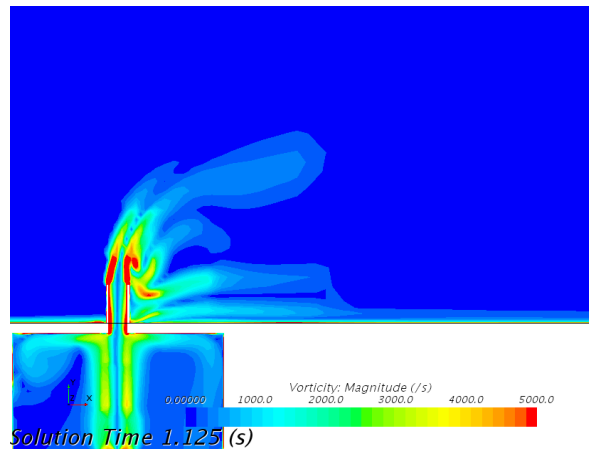


Figure 10: Contours of the axial mean velocity at the mid-section plane for pipe-jet.

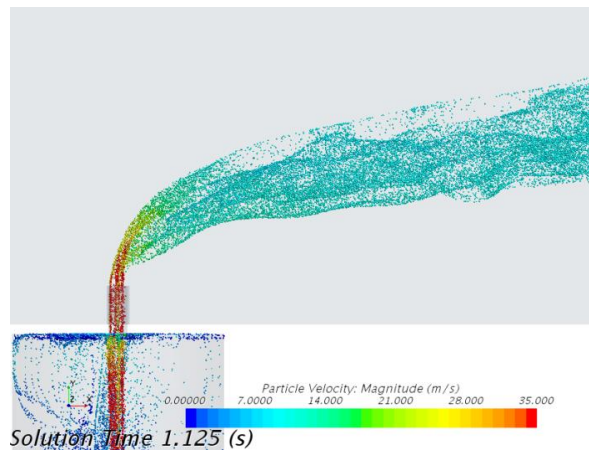
Comparatively figures 11 and 12 show similar results to figures 8 and 9 but for the jet with cavity. Results are taken at 1.25 sec. computational time. The mean velocity and vorticity contours and velocity vector plot within the cavity are shown in figure 13. A difference in midplane velocity is observed at the inlet and outlet of the cavity. A mass balance analysis was conducted and found that the mass flowing into the cavity matched the outgoing flow. The L/θ was calculated to be 444.33 for the cavity indicating a possibility of oscillation. As compared with the jet without cavity, reduced velocity, initial jet penetration and vorticity are seen in the near jet outlet. The particles' velocity plot is more distorted with reduced slope. Since pulsatile flow is expected, these results do not show an increase in jet penetration due to pulsation which is an indicator that the pulse is not being produced by the jet cavity at an optimal amplitude and frequency as seen by Eroglu (2001) and Coussement (2012).



(a)



(b)



(c)

Figure 11: Axial contours of (a) mean velocity, (b) vorticity and (c) particle velocity for the pipe-jet with cavity.

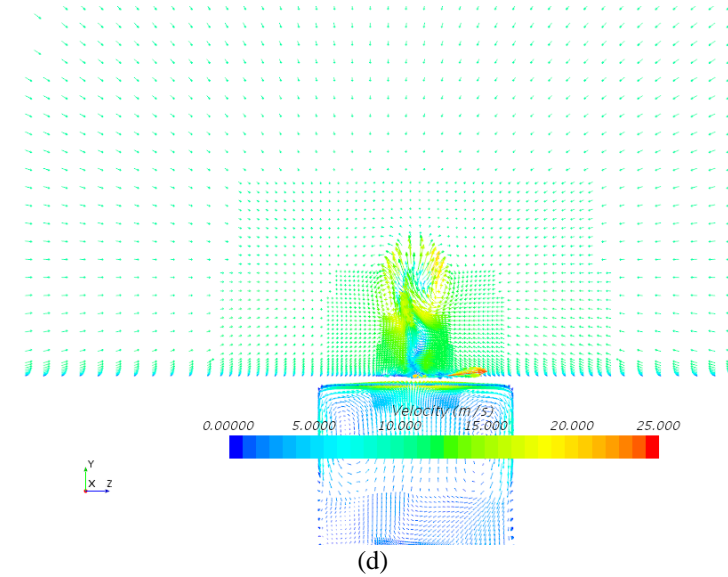
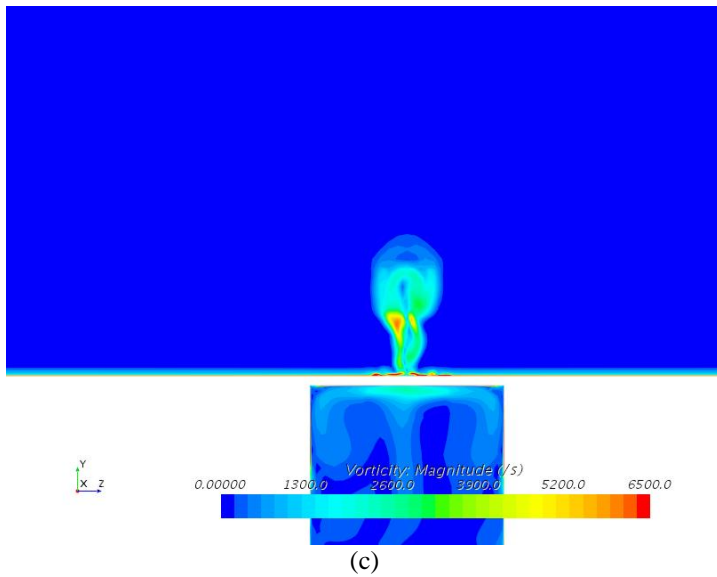
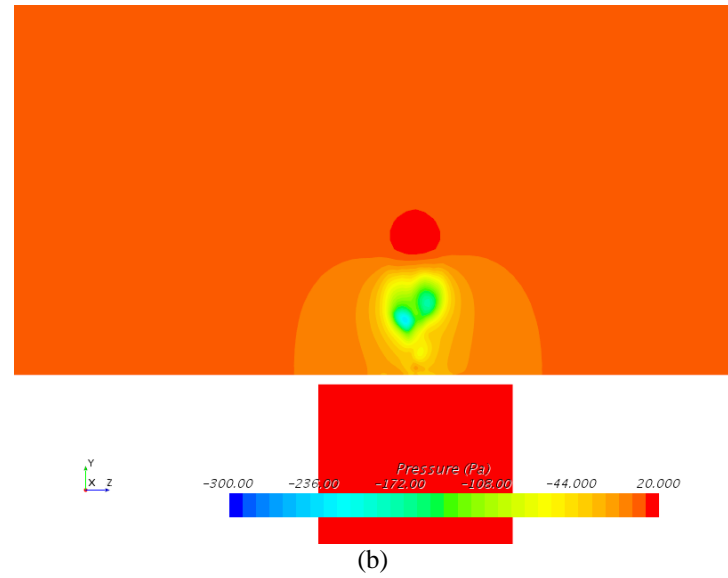
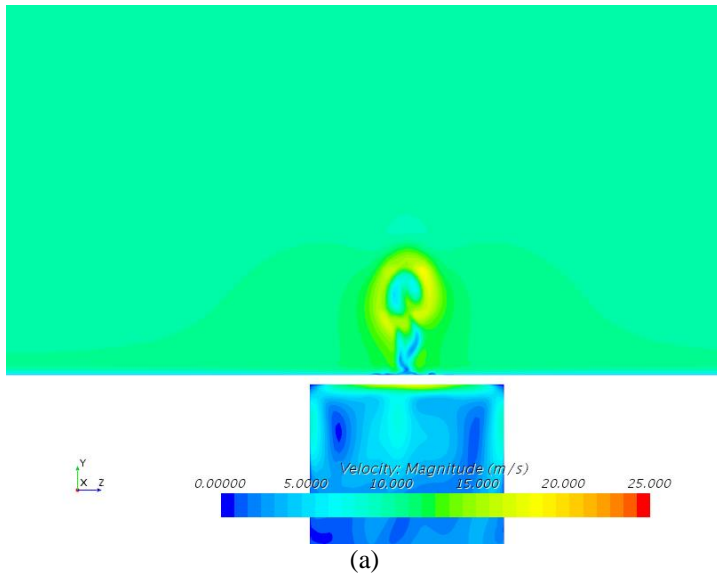
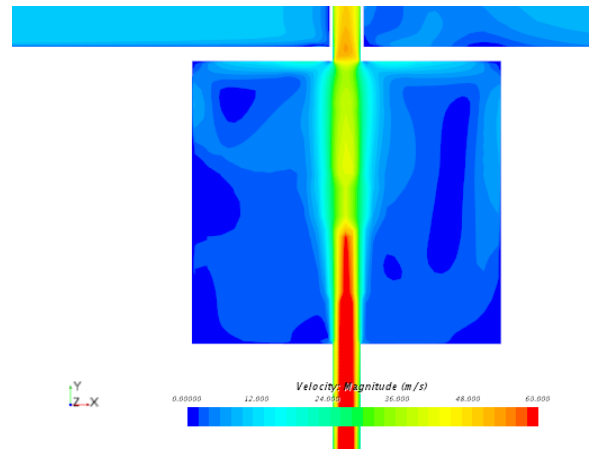
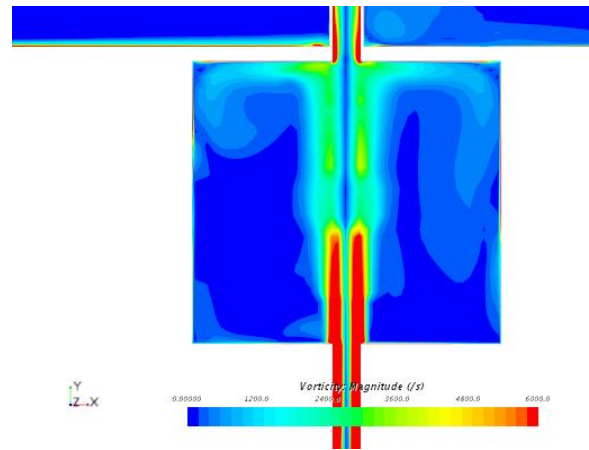


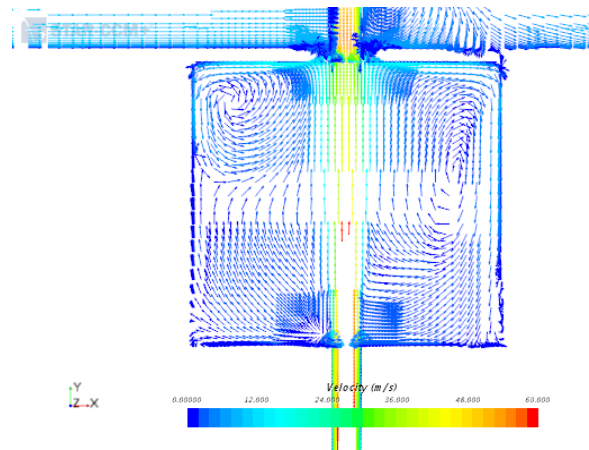
Figure 12: Spanwise contours of the (a) mean velocity, (b) pressure, (c) vorticity, and (d) velocity vector at $x/d=1$ for the pipe-jet with cavity in crossflow.



(a)



(b)



(c)

Figure 13: Contours of the (a) mean velocity and (b) vorticity, and (c) velocity vector within the cavity.

The counter-rotating vortex pair is still developing at $x/d=1$ with reduced strength which indicates the presence of cavity has resulted in increased mixing and reduced jet's momentum and penetration. The reduced jet trajectory can be a result of the non-optimal pulsation strength and frequency produced by the cavity.

Formation of vortices inside the cavity is observed and more pronounced in the left hand side for this time step. The left hand side has a single vortex occupying the downwind half of the cavity and no indication of the secondary or ternary vortices on this side, while the right side has a large vortex that almost occupies the whole cavity. The asymmetric vortices on the left side and right side may indicate instability in the cavity leading to oscillations. However, the vortices on the left and right side impinge on the pipe flow which can be the feedback system for generating oscillations. The mean velocity of the pipe at the cavity is narrowed due to impingement and reduced vorticity is observed at this location.

An increased vorticity in the pipe near wake and immediately downstream of the pipe-jet outlet is observed. Multiple burst of vortices downstream of the pipe-jet outlet could be the result if low speed pulsations, emanating from the jet, moving downstream as seen by Sau (2010).

Figure 14 shows the axial mean velocity profiles along the mid-section plane for the jet with cavity for different periods, at different axial locations. At $x/D=0$, at all periods, the peak velocity reaches at slightly below 5 cm above the zero elevation (here zero elevation corresponds to tube outlet) with a smaller peak below. Above the peak velocity, the profiles drop to a value less than 10 m/sec, before it increases and approaches the crossflow mean velocity. The profiles are associated with the initial jet ejection and tilting into the crossflow with initial deformation for the formation of counter rotating vortex pair (CVP). At further downstream locations, the peak velocity profiles narrow and the smaller peaks are distorted and broaden with time which grow to distinctive peaks, before appearance of additional peaks near zero elevation. The two velocity peaks seem to correspond to two distinct vortices, one due to pipe jet shear layers into crossflow and the smaller one due to the impingement of the recirculating flow within the cavity,

creating oscillation with a broad frequency range that follows the initial vortex. While the initial shear layer vortices deform to form CVP downstream, the oscillatory flow follows suit with similar behavior. The addition of vortices due to oscillation should enhance the mixing process.

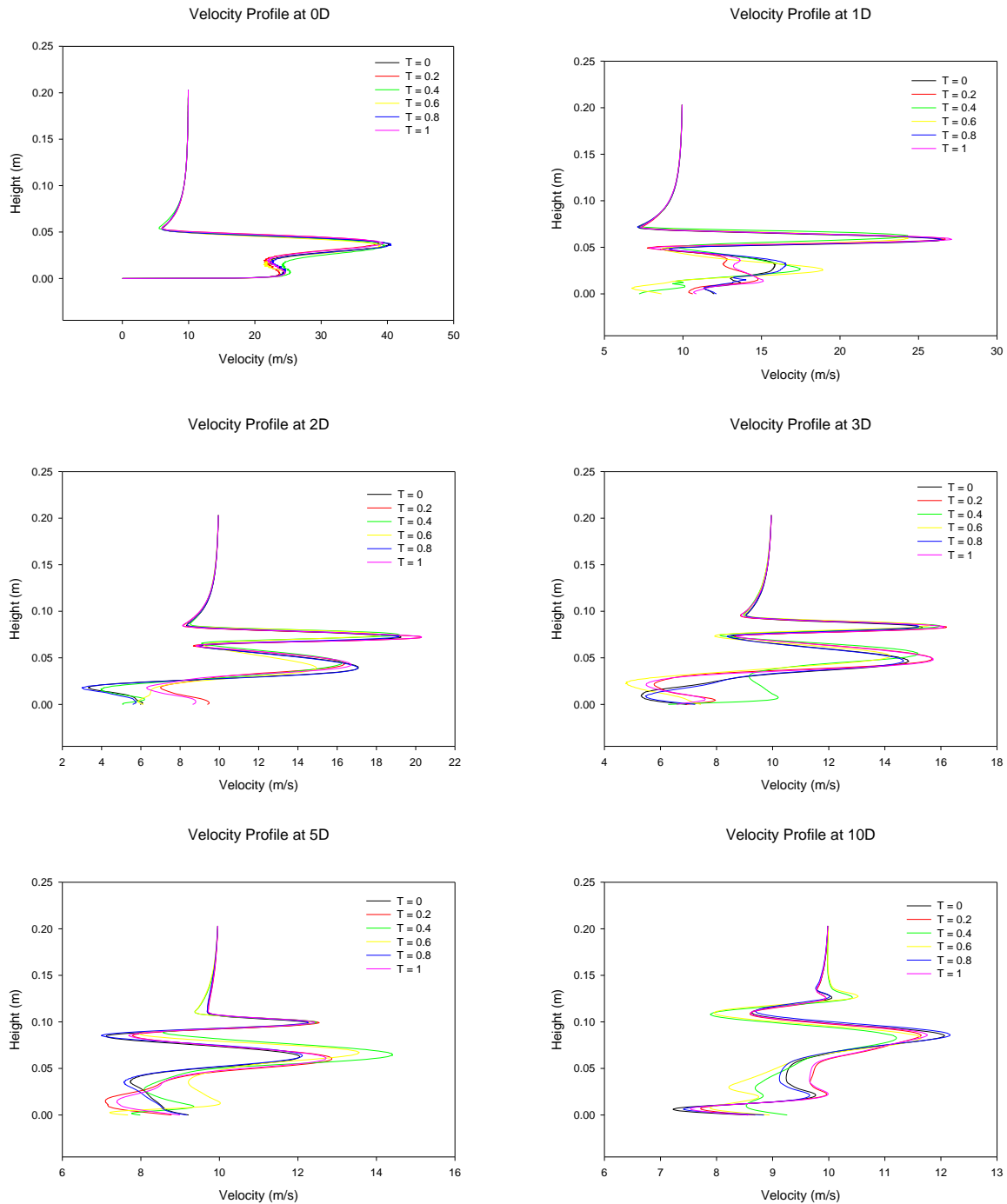


Figure 14: Axial mean velocity profiles along the mid-section plane.

At $x/D=5$ and 10 , the primary vortices have lost their strength significantly due to an increased entrainment and the secondary vortices become dominant, with appearance of additional smaller peaks below are due to additional oscillatory vortices.

Figures 15 shows samples of spanwise vorticity contours at different axial locations for different periods for the pipe-jet with cavity. The figure also includes vorticity contours for the pipe-jet as well. Results for the pipe-jet shows the shear layers from the pipe and the formation of the counter-rotating vortex pair which is well established at $x/d=3$. For the jet with cavity, there are also shear layers emanating from the tube, stretch and fold, to form a nearly symmetric CVP which is distinct at $x/d = 5$. With increasing time, the shear layers are distorted and there is initial mingling of these shear layers which is more distinct for $t = 0.3P$ with the formation of CVP at $x/d = 5$. The areas below the CVP indicate trailing vortices which are more distinct at $x/d=5$.

Within the round cavity, there are recirculation regions, before the pipe exit that impinge on the pipe flow, creating oscillation. The period of impingement seems to be between $0.2-0.4$ sec., corresponding to a Strouhal number ranging between 0.0028 to 0.0056 . The Strouhal number is defined as:

$$St = \frac{f*d_j}{U_{o,j}}, \quad (7)$$

where f is the oscillation frequency, d_j is the diameter of the pipe-jet outlet and $U_{o,j}$ is the velocity at the exit of the pipe-jet. These values are in agreement with the previous results (Johari 1999) for low duty cycles.

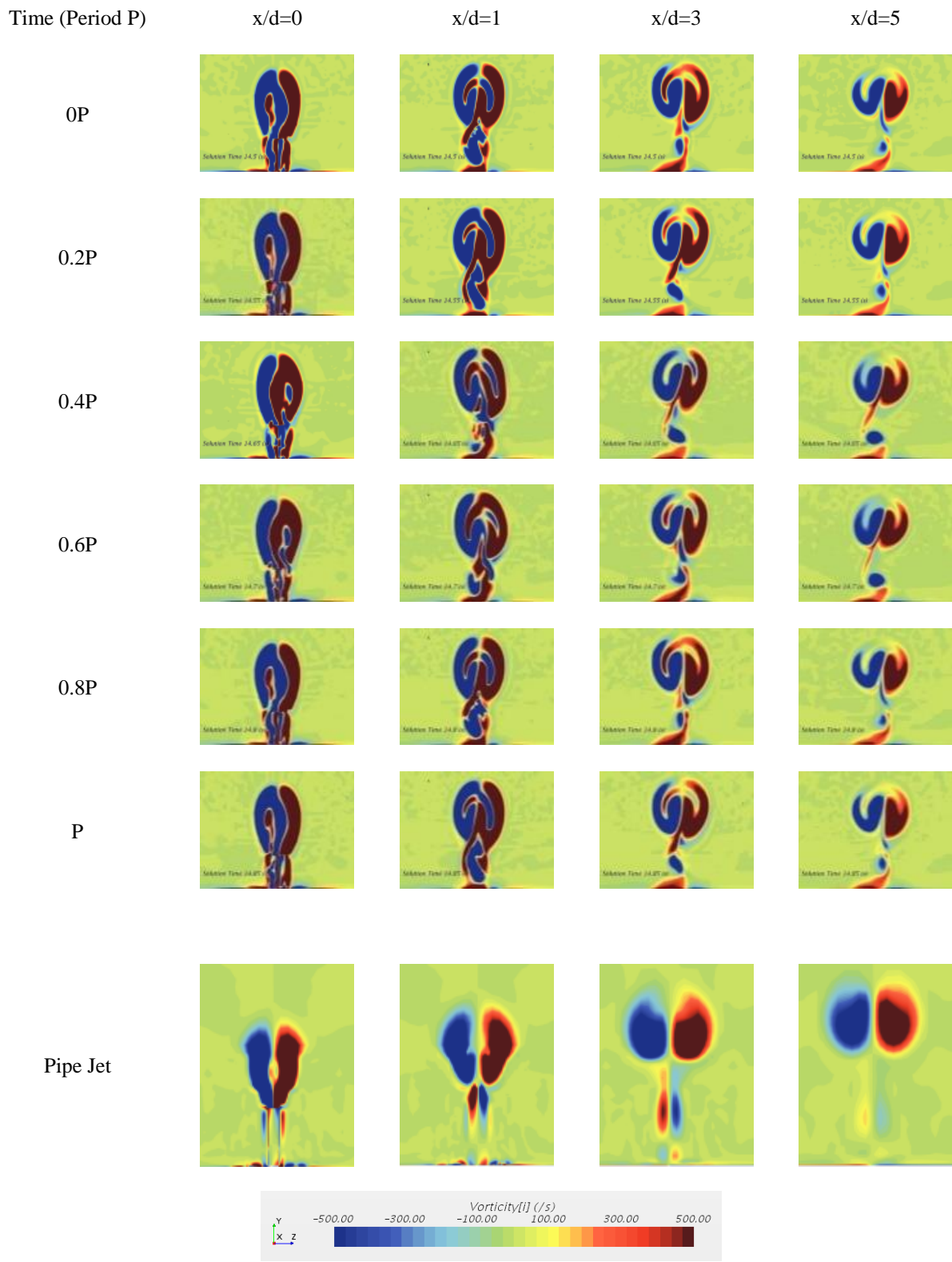


Figure 15: Spanwise vorticity contours

Figure 16 shows the trajectory of the JICF. Figure 16 shows the coefficients of the trajectory equation as:

$$\frac{y}{d} = a \left(\frac{x}{d} \right)^m \quad (8)$$

The trajectory is obtained by finding the location of maximum velocity at each axial location for each period. For the pipe-jet without cavity, beyond $x/d=1$, the trajectory and the power-fit curve are nearly identical with the slope and intercept values of respectively 0.40 and 3.00. These values are nearly identical to our previous investigations (Phan and Rahai 2005). However, when the cavity is added, the instantaneous trajectory changes significantly. For $t = 0-0.6$, the trajectory peaks at approximately $x/d = 2.5$, is minimum at approximately $x/d = 4.2$, before it increases again with some variations in the slope. For $t = 0.8$ and 1.0 , the peak velocity is observed at approximately $x/d = 5$ and becomes a minimum at approximately $x/d = 6.2$, before the lines increase with nearly the same slope. These variations are associated with passage of vortices emanated from the tube at different times. It shows that for large periods, another puff of vorticity ejected from the tube with higher strength and thus higher penetration. Thus, beyond the initial axial location where the trajectory shows lower penetration than that of the jet, with pulsation, the penetration is increased significantly. The cavity jet trajectories were split into two time averaged curves. Unlike the pipe-jet where the velocity profiles have single maximum valued peaks, the velocity profiles for the pipe jet with cavity exhibited two distinct peaks that identifies the jet splitting into a high and low stream as it progresses into the crossflow. The maximum points of the peak were separated into minimum and maximum jet trajectory profiles and fitted with power fit curves. The maximum jet trajectory is a result of the increased penetration from the vortex rings generated from the oscillatory flow. The minimum jet trajectory is the flow that follows the vortex rings and has the trajectory of similar to the pipe jet. This behavior of the min and max jet trajectories are in agreement with Johari (2006) on the comparison of the pulsed and steady jet.

Table 1 also includes approximate variations of the power law fits. The intercept coefficient for jet with cavity is more than 53% higher than that of the jet without cavity, while the slope is less which indicate while pulsation increases penetration, increased mixing reduces the slope.

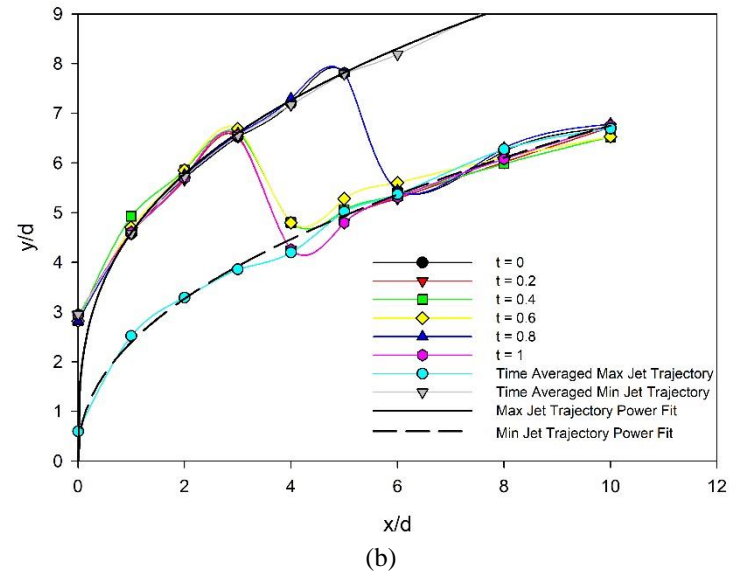
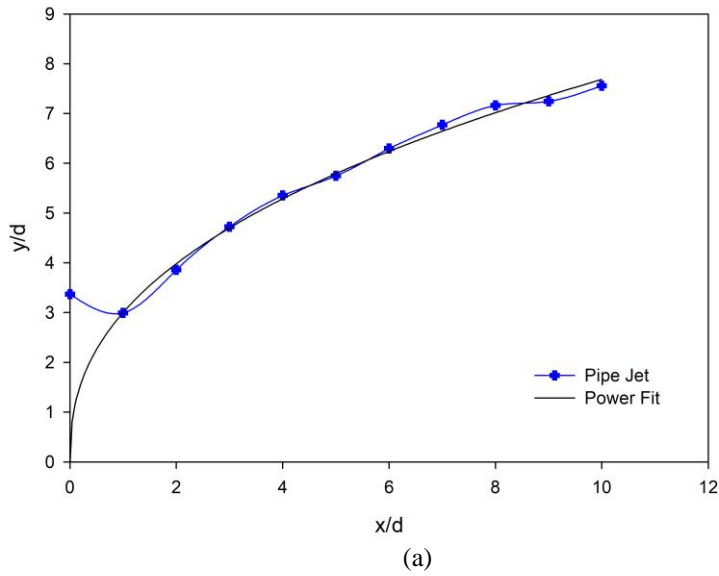


Figure 16: Jet trajectory, (a) Pipe jet, (b) Pipe Jet with cavity

Power Fit Coefficients				
	Pipe Jet		With Cavity	
			Min.	Max.
a	3.00		2.39	4.60
m	0.41		0.45	0.32

Table 1: Power coefficients.

Part 2 - Experimental

Experimental Setup

Figure 17 shows the experimental set-up. The experiments were carried out in a low speed open-circuit wind tunnel which consists of seven main components: the motor, blower, diffuser, settling chamber, contraction, adaptor and test section. Air is driven through the tunnel by a New York Blower Company General Purpose Fan, which is a 3750 CFM backward airfoil type, powered by a 5 HP electric motor. The diffuser is a two-part diffuser expanding from 43.2X63.5 cm to 76.2X76.2 cm over a distance of 91.4 cm. Boundary layer control is generated by a screen with open area ratio of 62.4% placed across the flow at the middle of the diffuser. The diffuser section is followed by the settling chamber which has a hexagonal honeycomb (3.8 cm deep with 3.2 mm cells) and three screens with open area ratios of respectively 62.4%, 59.1% and 59.1%. Following the settling chamber is a 3-D contraction with a 10:1 area ratio over a distance of 91 cm. Following the contraction, an adaptor is used to transition to the test section with cross section of 30.48 cm x 38.1 cm over a distance of 76.2 cm. The test section is 213.36 cm long. In the range of 3 to 45 m/s, the mean velocity varies by less than .5% and at all speeds; the background intensity is less than 0.2%. The boundary layer for the experiment is controlled by using a flat knife edge plate facing the flow with a distance of 5.88 cm from the start of the test section. The flat plate top surface is elevated 5.715 cm from the bottom of the wind tunnel.



Figure 17: Experimental setup

The jet system consisted of a Gast centrifugal air pump with a 1.8 HP motor and a maximum flow rate of 27 CFM. The pump is connected to a plastic container which acts as a settling chamber with dimensions 81.28cm x 60.96 cm x 53.34 cm (Length x width x height). From the settling chamber a round pipe with and without cavity are attached. The round pipe with an internal diameter of 1.27cm exits perpendicular to the cross flow and is placed 13.95 cm from the leading edge of the flat plate. The jet exit is 10.16 cm for the pipe jet and 2.54 cm for the jet with cavity above the bottom of the wind tunnel floor. The cavity dimensions were 6.36 cm long and 13.97 cm respectively in length and diameter.

The experiments were carried out at the wind tunnel free stream mean velocity of 10 m/sec. and pipe jet mean flow ratio of $r=4$. The jet diameter and pipe penetration distance for the pipe jet in crossflow are the same dimensions as the numerical investigations. Due to physical constraints of the wind tunnel, the dimension for the cavity driven oscillatory jet in cross flow needed to be altered. The pipe exiting the cavity and penetrating into the cross flow was increased to $5.5D$ and the pipe penetrating into the crossflow by $1D$. Axial time averaged mean velocity and turbulent velocity were measured with a Measurement Science Enterprise Inc. (MSE) 1-D Mini Laser Doppler Velocimetry (LDV) probe. The probe was able to move in axial and vertical directions by using a two dimensional Velmex Bislides traverse mechanism with a resolution of 0.0635mm. Measurements were carried out in a plane at the midsection of the jet profile. Measurements were taken at $x/d = 1,2,3,4,5,6 \text{ \& } 7$ where d is the jet diameter and the origin is located at the downstream inner edge of the pipe exit. At each measurement location, over 1000 samples were taken and analyzed at a sample rate of 2048 samples per second using the MSE provided software.

For LDV measurements, ROSCO vapor plus fog was used as the seeding particles. The fog was piped into the inlet of the blower fan for the wind tunnel and air pump for the jet. The fog density was adjusted to allow optimal signal output from the LDV.

Results & Discussions

Figure 18 depicts the profiles of axial mean velocity for the pipe jet in crossflow. The pipe jet shows a large rounded spike for $x/d = 0$ and the initial velocity is 0 at $y=0$. As the x/d distance increased, the flow in the wake region begins to fill in and an increase in velocity is seen. Also with the x/d distance increase, the maximum velocity spikes move in an upward trend indicating the growth of jet trajectory.

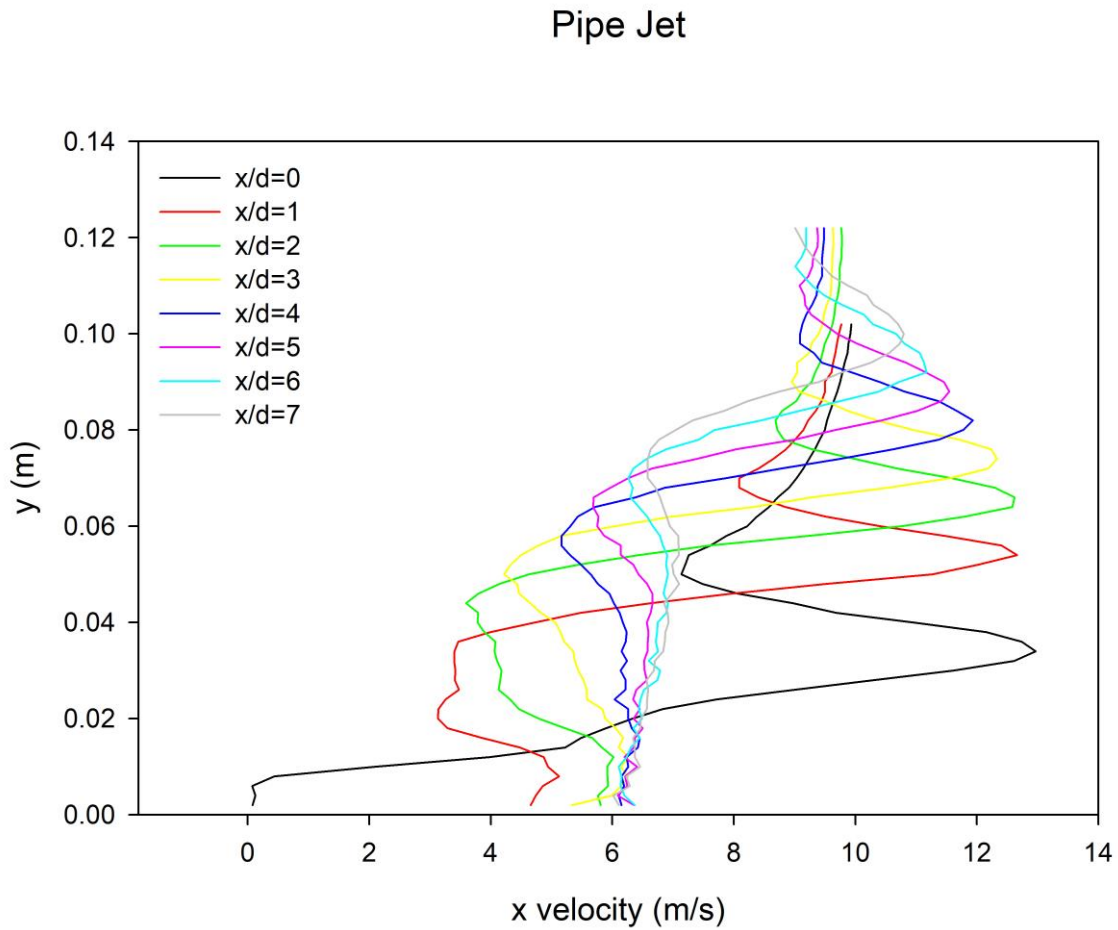


Figure 18: Axial mean velocity of Pipe Jet Experiments

Figure 19 shows the axial mean velocity profiles for the jet with cavity flow. The profiles are more closely spaced and are closer to the flat plate, when compared with corresponding profiles for the jet

without cavity, indicating reduced penetration of the jet in cross flow. The peak mean velocity magnitudes are less than those for the pipe-jet, indicating increased mixing for the jet with cavity.

Pipe Jet with Cavity

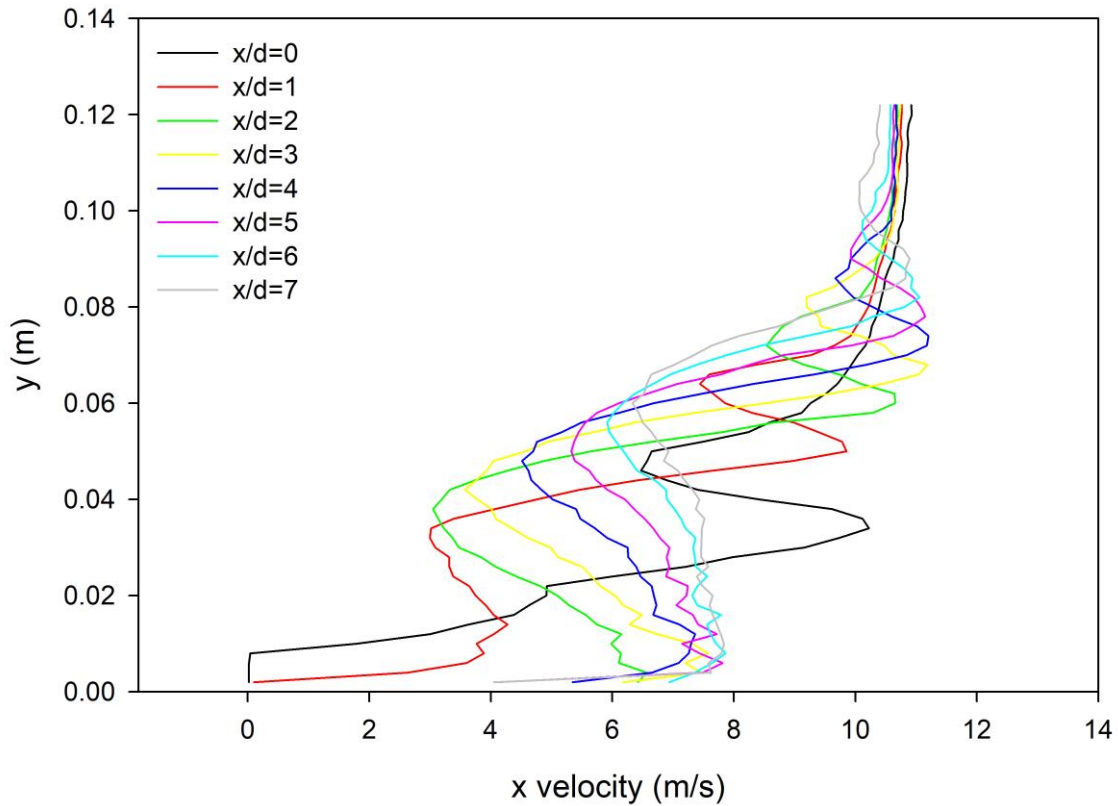


Figure 19: Axial mean velocity profiles of Jet with Cavity Experiments

Figures 20 and 21 show the turbulence intensity for the pipe jet and pipe jet with cavity respectively. The pipe jet has an overall higher turbulence intensity as compared to the pipe jet with cavity. The lower turbulence intensity for the pipe jet with cavity is a result of the mixing inside the cavity. As the flow exits the cavity created turbulence is dampened and dissipated in the pipe before it expels into the cross flow.

Pipe Jet Turbulence Intensity

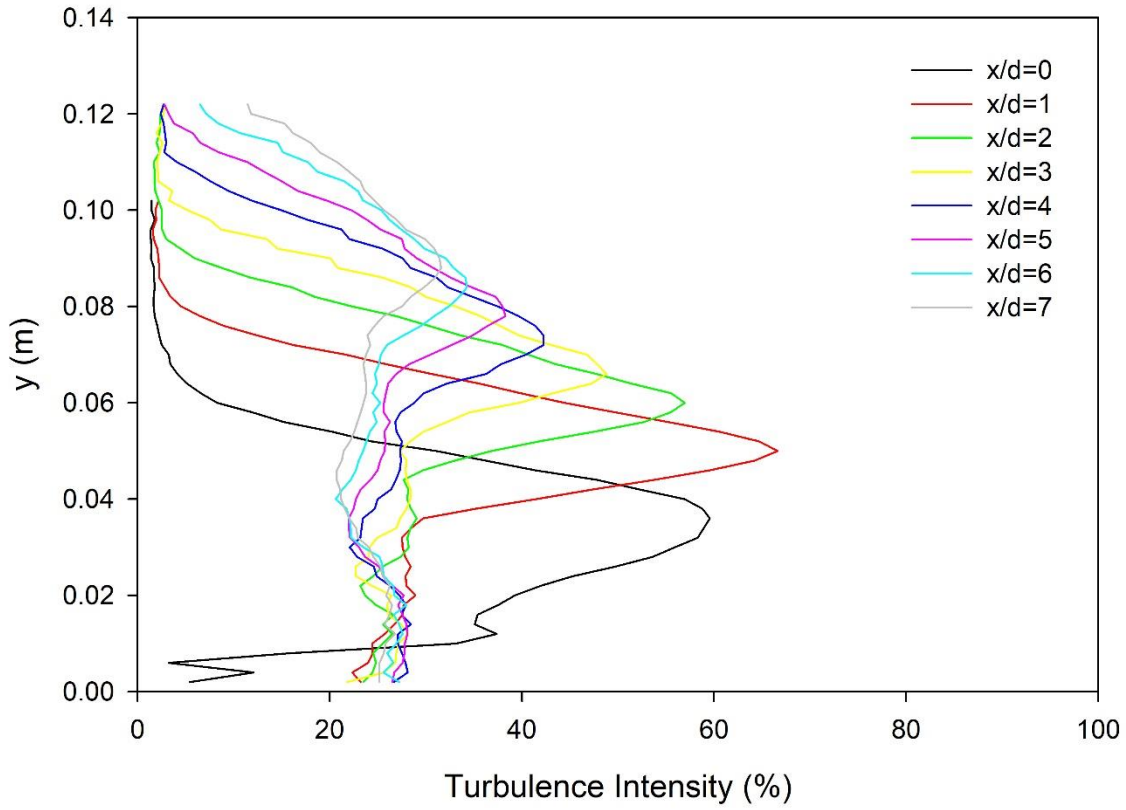


Figure 20: Axial Turbulence Intensity for a Pipe Jet

Pipe Jet with Cavity Turbulence Intensity

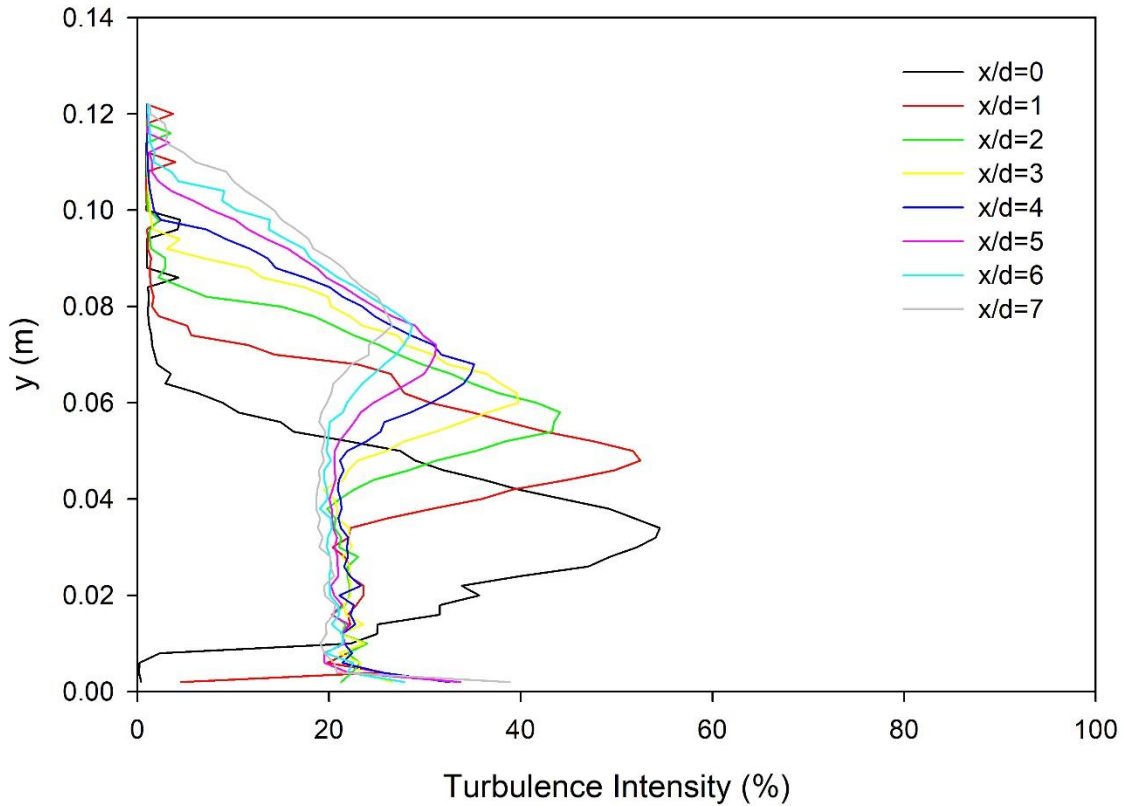
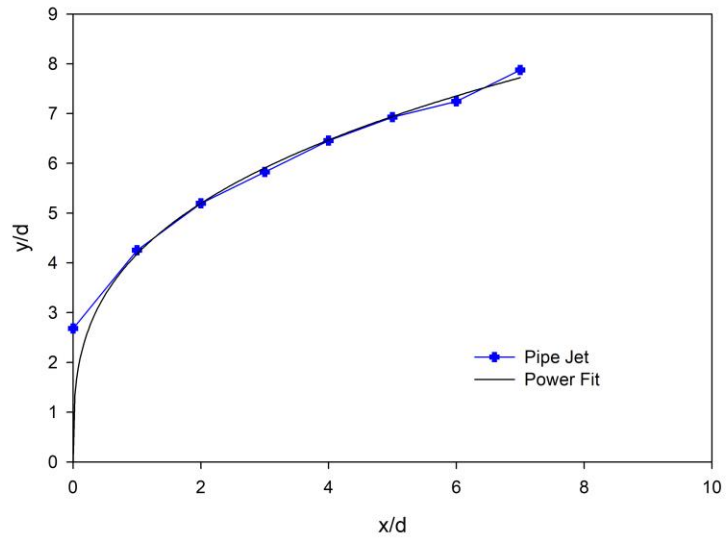
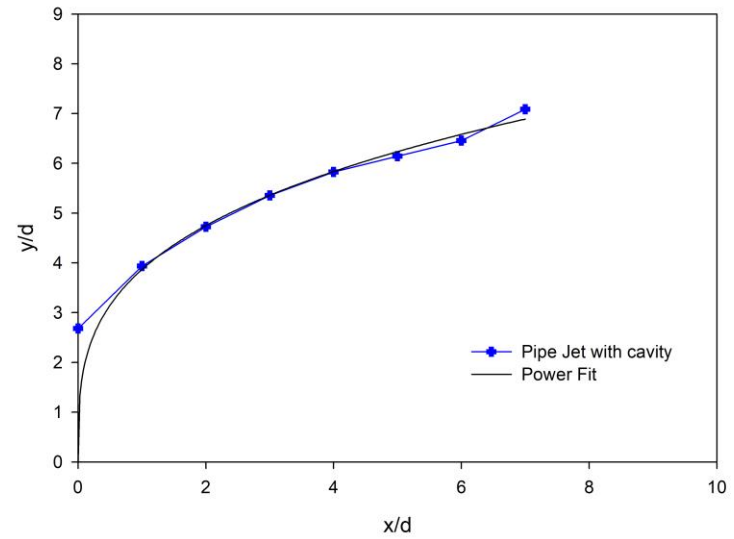


Figure 21: Axial Turbulence Intensity of a Pipe-jet with Cavity

Figure 22 shows the trajectory of both the pipe jet and the pipe jet with cavity along with a power fit curve and Table 2 shows the corresponding power coefficients using the same formula used in the numerical analyses. The intercept signifies the penetration rate while the slope is related to the entrainment and mixing. As can be seen, the penetration is reduced for the jet with cavity while the mixing is enhanced. When comparing these results with the corresponding numerical results, there are discrepancies. For the numerical results the mixing enhancement of the cavity-driven flow is much higher with higher penetration while in the experimental results the penetration is less than the plan jet penetration. The differences could be due to the measurement techniques, as LDV measures ensemble average while the numerical analyses were transient and could provide a range of values for the coefficients corresponding to the nature of the cavity driven flow.



(a)



(b)

Figure 22: Experimental Trajectory plots of (a) Pipe jet and (b) Pipe Jet with cavity

Power Fit Coefficients		
	Pipe Jet	With Cavity
a	4.18	3.87
m	0.32	0.30

Table 2. Experimental Power coefficients.

In order to capture the transitory characteristics of the flow, smoke flow visualizations were performed. Figure 23 shows comparisons of the profiles for the JICF with and without cavity. When analyzed for different times, the oscillations emitted from the pipe jet with cavity were not strong however slight alterations in the immediate wake regions could be seen.

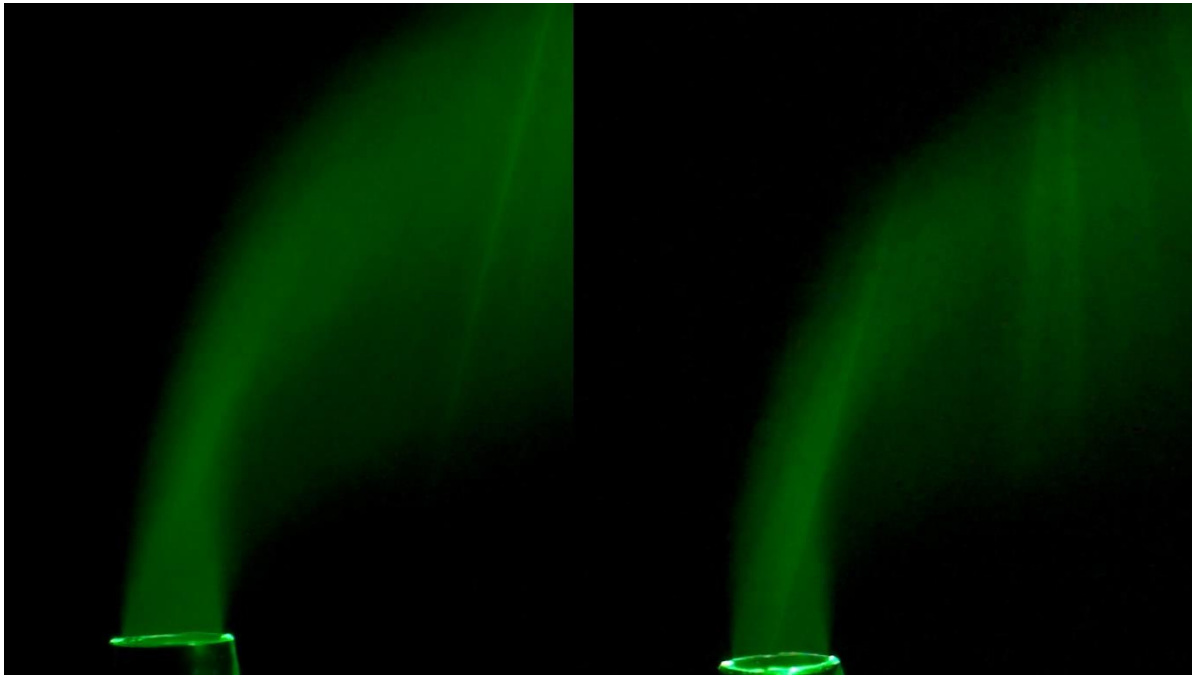
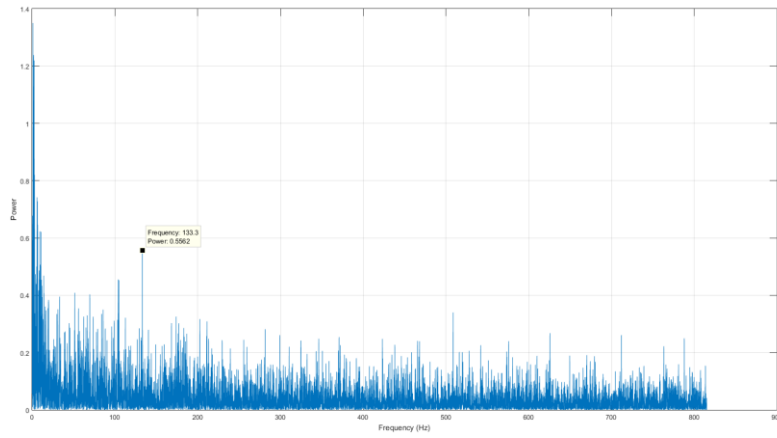
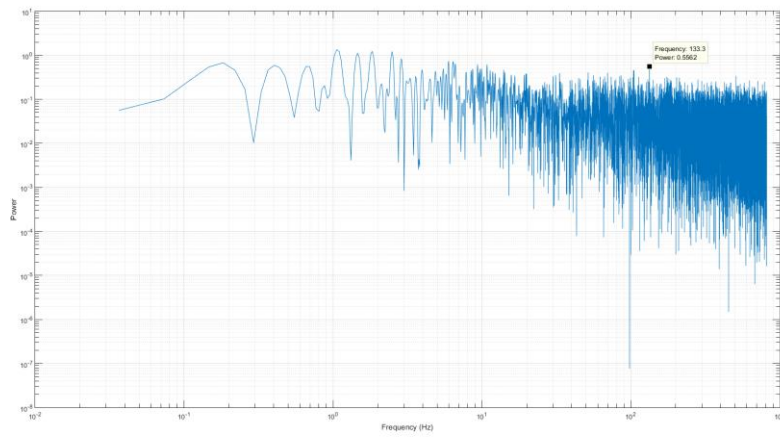


Figure 23: Flow of a Pipe Jet (left) and Pipe Jet with Cavity(right)

Figure 24 and 25 shows the power spectral density plot taken at $1d$ away from the jet exit along the center axis of the pipe for the pipe jet and pipe jet with cavity. The pipe jet has a weak frequency at 133 Hz. For the jet with the cavity, there are two dominant peaks at 66.68 Hz, 133.4 Hz and a smaller one at 200 Hz. The corresponding Strouhal numbers based on jet diameter for 66.68 Hz and 133.4 Hz are 0.021 and 0.042 respectively. Previous investigations on pulsatile jets in cross flow have indicated convective instabilities in the transverse jet shear layers at high jet to cross velocity ratios, r , which is strengthened with reducing r . It is a transition to a self-sustained unstable condition, where additional active excitation was not found to be effective in increasing the mixing rate.

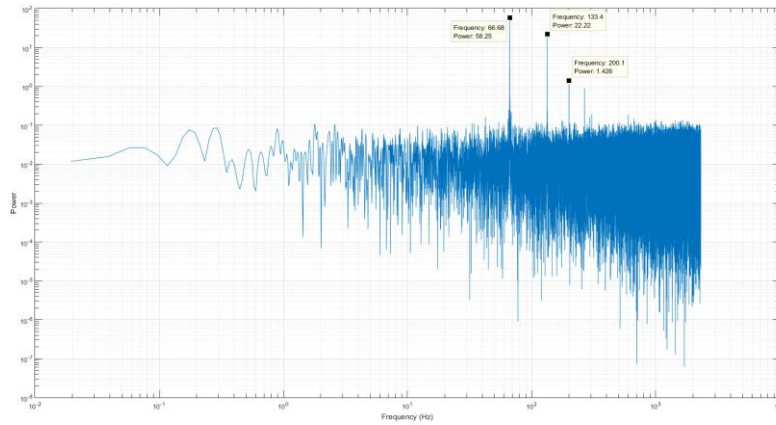


(a)

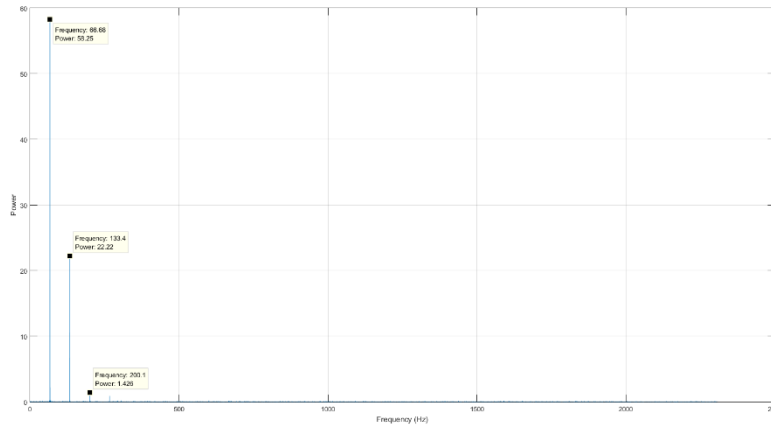


(b)

Figure 24: Power Spectral Densities for Pipe Jet in (a) Linear Scale and (b) Log-Log Scale



(a)



(b)

Figure 25: Power Spectral Densities for Pipe-Jet with Cavity in (a) Linear Scale and (b) Log-Log Scale

Power Spectral Density plots for $r=2$ and 3 indicate possible main peak of 39.68 Hz and 66.66 Hz respectively. Table 3 list the Reynolds number and Strouhal number for $r=2$, $r=3$ and $r=4$ and where the Strouhal numbers went from 0.025 to 0.027 and back down to 0.021 . The results do not display a linear relationship between Reynolds number and Strouhal number. The peak frequency increased from $r=2$ to $r=3$ and stayed the approximately the same at $r=4$. With a uniform peak frequency in $r=3$ and $r=4$, the decrease in the Strouhal number is due to the change in the mean velocity of the pipe-jet with cavity. The

effect of Reynolds number and Strouhal number for additional r values will be investigated in future studies.

r	Reynolds Number	Strouhal Number
2	168,000	0.025
3	252,000	0.027
4	336,000	0.021

Table 3: Variation of Strouhal Number with Reynolds Number

Pulsed jets could be divided into two categories. When the jet is strongly pulsed, the RMS velocity is much greater than the time-averaged mean velocity of the nozzle and the slug of fluid associated with each pulse is short, a series of vortex rings are generated that penetrated deeper into the cross flow. On the other hand, if the jet is weakly pulsed or the jet fluid slugs are relatively low then the mean jet penetration is not much different from an equivalent steady jet. Results from the PSD graphs indicate that the pulses are weak and the frequencies are distributed into a broadband spectrum for the pipe jet with cavity. This characteristics of the weakly pulsed jet of different frequencies emitted from the cavity exhibits that of the pipe jet without cavity.

Chapter IV

Effects of Oscillatory flow on the Human Respiratory System

Objective

Application of oscillatory flow in cavity can have an effect in the increased efficacy of inhaled medicines. The passive way of creating the oscillatory flow would simplify the device and also can increase mixing properties of the medicine into the flow stream. The effects of oscillatory flow on particles deposition in the human upper respiratory system were investigated numerically to see if a change of particle deposition was present. Numerical investigation of an oscillation flow and an airway model were assessed using the Computational Fluid Dynamics (CFD) software Siemens Star CCM+.

Background

Respiratory diseases and infections are commonly treated using inhaled medication preferably, due to the fast absorption on the large surface area of the alveolar region and the thin air-blood barrier (Hess 2008). The efficacy of the inhaled drug depends not only on drug itself but also on the level of deposition in the diseased/ infected region. Inhaled drug delivery flow through the respiratory system (fig 26), starting at the oral or nasal cavity in the nasopharynx region, travels through the tracheobronchial region and terminates in the pulmonary region. With an effective drug delivery system, oral administration is preferred due to the nasal cavity's effective filtering of the incoming flow (Laub 2017).

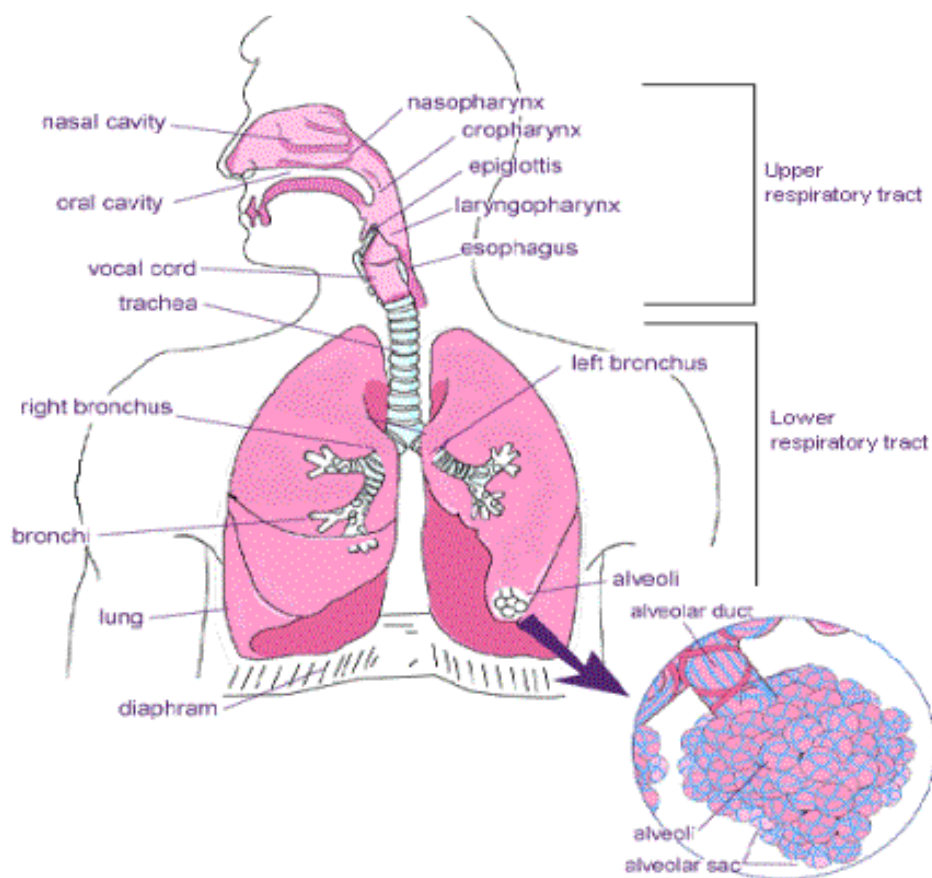


Figure 26: Respiratory System

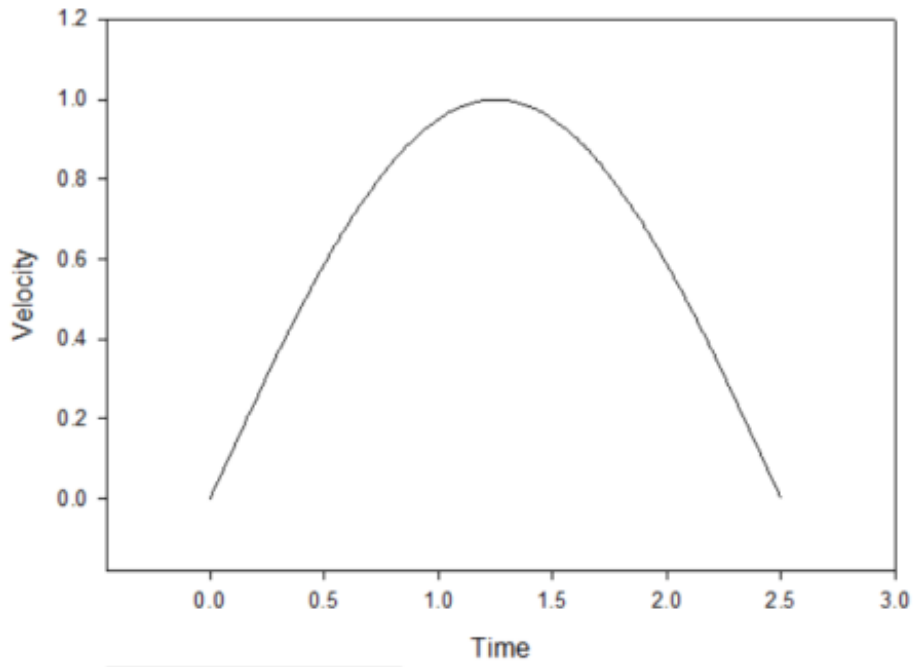
Particle deposition is influenced by particle size, inspiration and expiration rate, incoming flow conditions, airway geometry, and mucus along the airway. The effectiveness of the medication may be largely dependent upon the amount of medication that reaches the intended deposition site (Chow 2007). Large particles or droplets deposit by impaction in the upper respiratory tree of the lung (oropharyngeal and tracheobronchial region), where air velocity is high and the air flow is turbulent (Anderson 2005, Heyder 1982). Ruffin (1981, 1978) and Newhouse (1978) investigated the deposition of histamine aerosol in human airways, and concluded that the depositions were more effective in larger airways than if spread throughout the lung. This suggests that the larger airways are the main location for the receptors of histamine. Labiris & Dolovich (2003) have shown that the efficiency of the drug delivery and therapy may be compromised if the pharmaceutical aerosols are administrated to an unintended location of the

respiratory system. In asthmatic patients, the inflammatory cells such as Lymphocytes are uniformly distributed in the large and small airways (Heyder 1982) and they suggested that the efficiency of drug delivery would be increased and be more beneficial if the inhaled medicine is distributed throughout the entire lung. The most effective location for deposition of therapeutic aerosolized antibiotics or medical particulates is highly dependent on the type of infection and disease being treated.

Inhalers, nebulizer, and mechanical ventilation are means of delivery for solid and aerosol inhaled medicines. These devices are studied and optimized to effectively deliver medicines to the intended area. Particle deposition is analyzed through clinical trials using computed tomography (CT) scans (Cohen 2008, Conway 2012 and Newman 2006) and 2D gamma scintigraphy (Conway 2012, Newman 2006, Usami 2005 and Bondesson 2003). The delivery methods and particle sizes have been assessed through these studies (Usami 2005, Bondesson 2003 and Van den Berg 2012). In development of a drug delivery device and the understanding of particle deposition, previous studies involving particle flow on a diseased trachea have been studied (Taherian 2015, 2017).

Studies of the effect of oscillatory flow on particle in the respiratory system has been performed and presented at the 69th annual meeting of the American Physics Society Division of Fluid Dynamics in Portland, Oregon. The preliminary analysis was of a patient specific trachea along with 8 generations of airway branches. Inlet flow velocity was oscillated. The analysis used an oscillatory sinusoidal flow and superimposed it onto a normal breathing sinusoidal flow (fig 27) representing an acoustically driven oscillatory flow.

Inhalation Cycle



Oscillation Graph

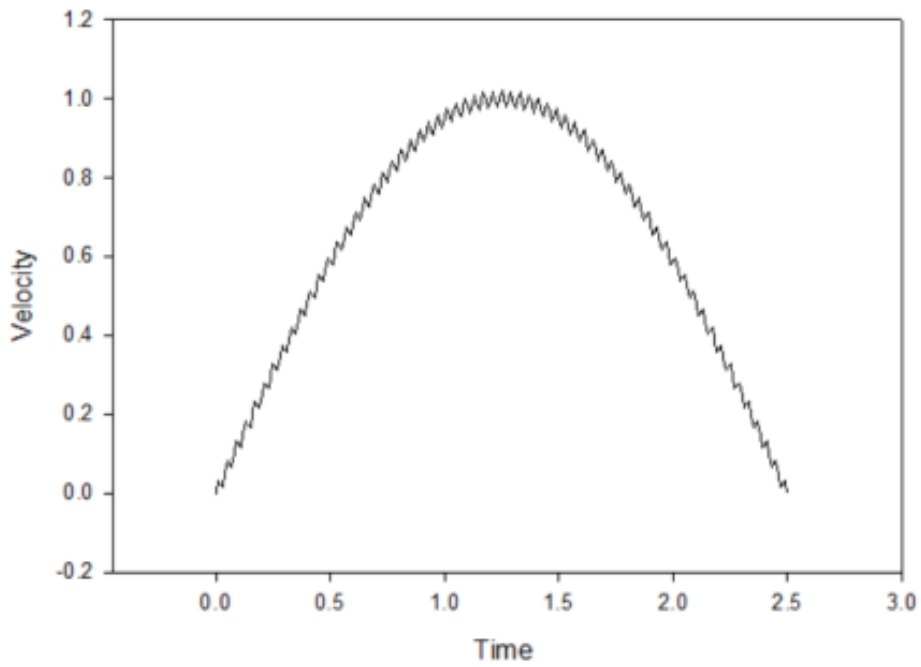


Figure 27: Inhalation and Oscillation Velocity Curve

Numerical Analysis

A 3-D model (fig 28) which was generated from 3-D doctor using de-identified publicly available CT scans, consists of 1 inlet (the trachea) and 51 outlets of up to the 8th generation which lead further into the lungs. The model was used for different scenarios of URANS analysis of oscillatory flow. The oral manifold was not used in this model since the amount of effective particle deposition in the airways depends on the particles that have exceeded this section. In realistic conditions, with the addition of the oral manifold, the flow is altered and not uniform at the entrance of the trachea. Another factor that affects the flow is the change of the airway shape during inspiration and expirations. To better assess the upper respiratory system, FSI and morphing techniques need to be implemented in addition to the oral manifold. However, a basic understanding of the particle mechanics inside the upper airway can be obtained by simplifying the problem if having a rigid upper airway.

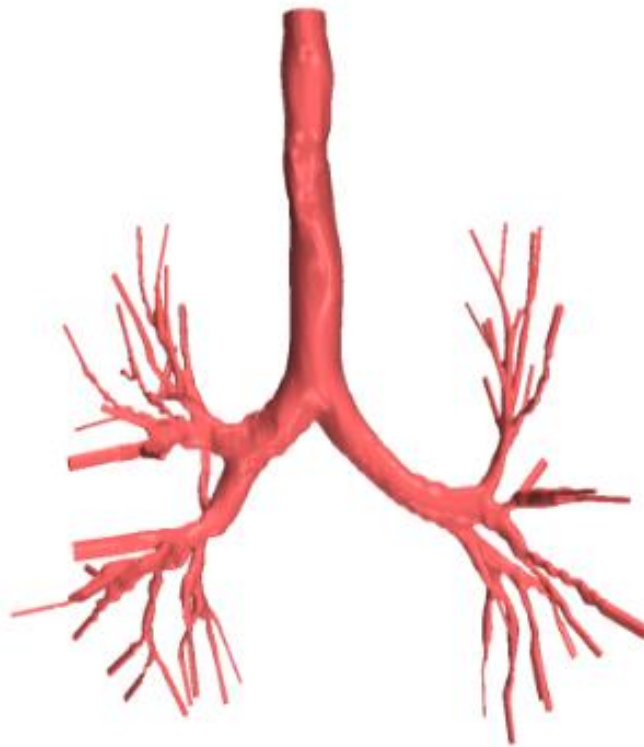


Figure 28: 3D Trachea Model

The mesh of the model consisted of a polyhedral mesh with prismatic inflation to resolve the boundary layers. Mesh independency was performed to select an optimal mesh size by running a course, medium, and fine mesh for the model. Velocity and pressures at selected points were compared to be less than 2% variance resulting the mesh is independent.

The boundary conditions for the models were a velocity inlet (at the trachea) with a pressure outlet (at the bronchioles). Inspiration lasting 2.5 seconds was only analyzed in this study since particle penetration to higher generation can result in an increase in medicine efficacy. The outlet boundary condition was assigned to be a split mass flow outlet (with each branch flow restricted lobar volume changes and outlet area ratios).

At the inlet, particles were injected uniformly across the surface. The particle trajectory and deposition patterns in the airways were analyzed. The particles selected were PM1 and 2.5 spherical carbon with a density of 1200 kg/m³. The simulation is a Lagrangian transport model with Schiller-Naumann equations resolving the drag coefficient. The walls have particle stick conditions applied. The particle inlet velocity was selected as the same, in contrast to the inlet air flow conditions.

The CFD scenarios of inlet conditions were analyzed as seen in fig 28. The first set of simulations involved the particles injected into the flow with the inlet non-oscillatory and particle velocity oscillatory (velocity mismatch). The second set consisted of the particles and inlet airflow having matched oscillatory velocities. The flow of air and particles were governed by:

$$V(t) = A_1 \sin\left(\frac{2}{5}\pi t\right) + A_2 * \sin(2\pi ft)$$

with V = velocity, t = time, A₁ = Maximum Breath velocity, A₂ = Oscillation Flow Amplitude, and f = Oscillation Frequency

Inhalation and velocity particle mismatch consisted of the particle oscillation velocity amplitude of 1/50th of the maximum inhalation velocity. The frequencies chosen were 50Hz and 300 Hz.

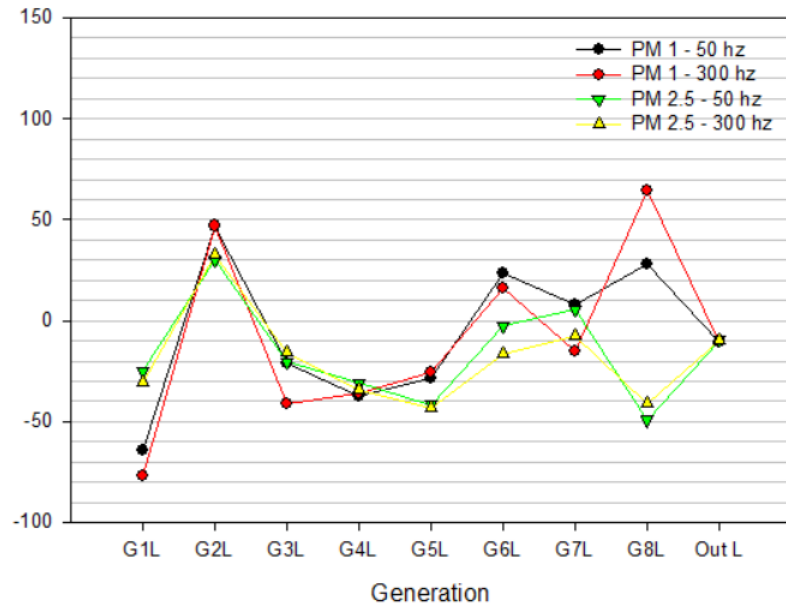
The second method consisted of a match of inhalation inlet velocity and particle injection velocity. Part one of the velocity match was the analysis of different oscillation frequencies (which were chosen to be 50, 100, 300 and 600 Hz with a set oscillation amplitude of 1/50 of the inlet velocity). In part two, with 600 Hz being the optimal frequency found in part one, the amplitude was compared between 1/50th and 1/25th of the inlet velocity.

The flow inside the upper airways is largely due to the complex geometry. In addition, the flow at the branching and reduced airway diameters may be either laminar or turbulent depending on the location and time.

Results & Discussions

Each comparison of particle deposition is between a single inspiration with a normal sinusoidal breath. For the velocity mismatch depositions, fig 29 shows that there are slight percentage changes when comparing PM1 and PM2.5 for 50 and 300hz oscillation frequency. The percentage change allowed for an increase in deposition in the 1st generation on the right-side branch and a decrease in the left branch. In the 3rd, 4th, 5th and 6th left-side branch and the 4th, 5th, 6th and 7th right-side branch, there were also decrease in particle deposition. In looking at the particles passing through the model, there is a decrease in the left and right side. This means that there is a redistribution and slight increase in particle deposition in the 1st thru 8th generations.

Left Side Lung Deposition Percentage Change of Mixed Flow to Uniform Inlet Flow



Right Side Lung Deposition Percentage Change of Mixed Flow to Uniform Inlet Flow

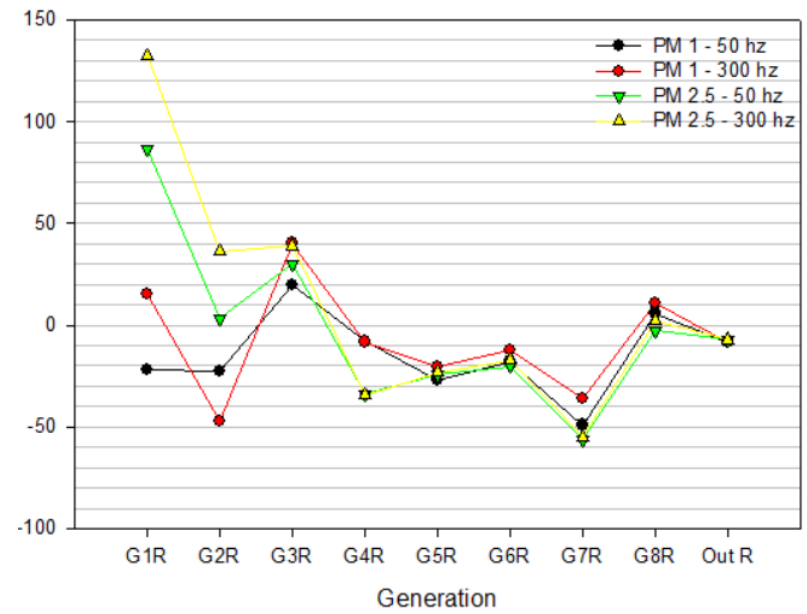
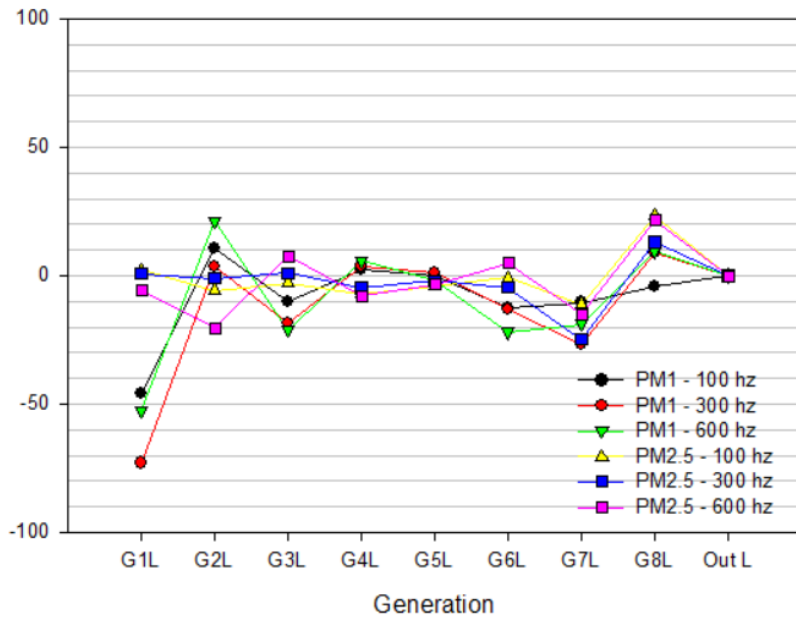


Figure 29: Percentage Deposition Change of Mixed Flow Comparison for the Left and Right Lobe

The analytical results for oscillatory velocity match where the inlet air velocity and the particles injected velocity matched as shown in fig 26. There is a greater redistribution seen in both the left and right sides. More particles were able to travel further down the generation on the right branch when the oscillatory flows were applied. On the left-side branch, there was a decrease in particle distribution. The largest redistribution frequency is 100 Hz for PM 1 and 600 Hz for PM2.5. When comparing the left and right-side outlet particle count, there is no change in the particles passing through these generations. It seems, therefore, that the oscillation has little effect on the PM 1 and PM 2.5 size particles.

The analyses for velocity also match, however, an amplitude change was applied in the final run (Fig 30). The amplitude was increased from $1/50^{\text{th}}$ to $1/25^{\text{th}}$ of the inhalation velocity. There is little to no effect when comparing the oscillation amplitudes as seen in fig 31. The largest percentage change is just under 1% and suggests that the oscillation had no significant change on PM1 and 2.5. The effects of amplitude change on oscillatory flow as related to other particle sizes and different frequencies needs to be investigated.

Percentage Difference for Left Airway Deposition with Comparison of 100, 300 and 600 hz to 50 hz



Percentage Difference for Right Airway Deposition with Comparison of 100, 300 and 600 hz to 50 hz

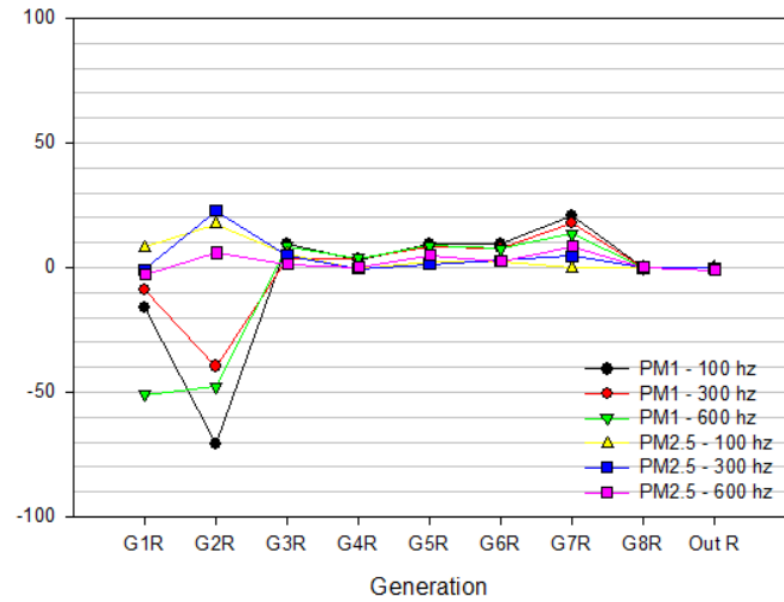


Figure 30: Percentage Comparison for Particle and Velocity Oscillation Matching Frequencies for the Left and Right Lobe

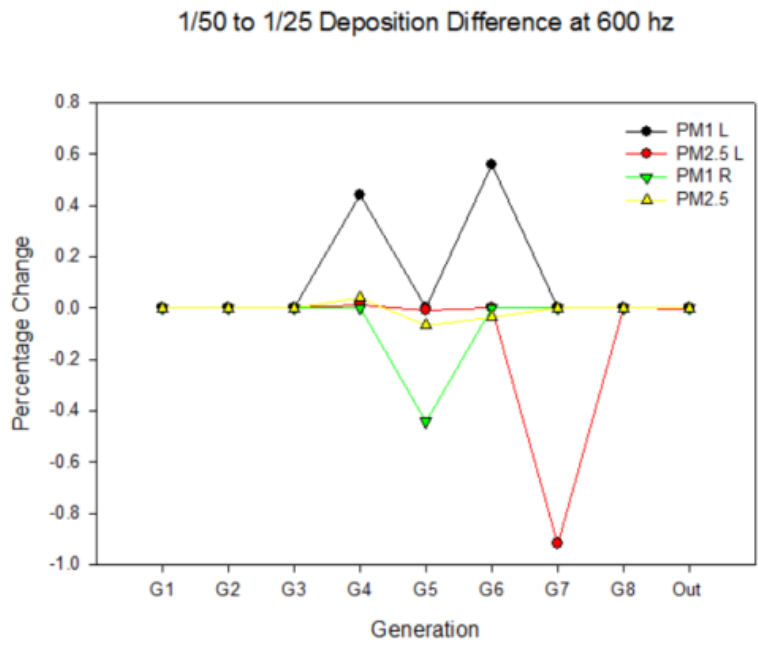


Figure 31: Comparison of Amplitude Change for both Left and Right Lobe

Chapter V

Conclusions

A cavity driven oscillatory jet into cross flow was investigated numerically using Siemens Star CCM+ CFD software and experimentally by LDV measurements. The cavity selected to generate the oscillations was an annular cavity geometry, with a length to depth ratio of 2 that produced a three dimensional oscillatory flow. The length of the cavity was 0.127 m and the inlet and outlet diameter of the cavity was 0.0127 m. The mean velocity of the crossflow was selected to be 10 m/s and the velocity ratio of $r=4$ was used resulting in a Reynolds number of 33,600 based on the jet diameter and for the cavity of 336,000 based on the length of the cavity. Numerical results indicated that the pulsed jet had a lower overall trajectory and an increase in mixing as compared to the steady jet in cross flow. There was also more dispersed vorticity in the cavity jet flow which contributed to the jet flow filling in the wake region sooner. Experiments were used to confirm the flow was oscillatory and from the power spectral density plots indicated the flow pulsed at 66.68 Hz giving a Strouhal number of 0.021. The pulse flow strength for the pipe jet with cavity were small and behaved similarly to a steady jet in crossflow with slight differences in the jet characteristics.

Numerical Investigations were also performed on the effect of oscillatory flow in the human upper respiratory system. The numerical model included the trachea and up to 8 generations of the lung. The inhalation cycle of 2.5 seconds was analyzed to determine how oscillatory flow affects the deposition rates of 1 and 2.5 μm particles in the lung. Results indicated that the oscillatory flow redistributed the depositions between the left side and right side and through different generations of the lung.

References

- Anderson, P. J. (2005). History of Aerosol Therapy: Liquid Nebulization to MDIs to DPIs. *RESPIRATORY CARE*, 50(9), 12.
- Basley, J., Pastur, L. R., Delprat, N., & Lusseyran, F. (2013). Space-time aspects of a three-dimensional multi-modulated open cavity flow. *Physics of Fluids*, 25(6), 064105. <https://doi.org/10.1063/1.4811692>
- Basley, J., Pastur, L. R., Lusseyran, F., Faure, T. M., & Delprat, N. (2011). Experimental investigation of global structures in an incompressible cavity flow using time-resolved PIV. *Experiments in Fluids*, 50(4), 905–918. <https://doi.org/10.1007/s00348-010-0942-9>
- Bensider, N., Amina, M., & Mohamed, A. (2017). Control of self-sustained jet oscillations in 3D thin rectangular cavity. *Chemical Engineering Research and Design*, 117, 533–541. <https://doi.org/10.1016/j.cherd.2016.11.012>
- Bondesson, E., Bengtsson, T., Borgström, L., Nilsson, L.-E., Norrgren, K., Trofast, E., & Wollmer, P. (2003). Planar gamma scintigraphy—points to consider when quantifying pulmonary dry powder aerosol deposition. *International Journal of Pharmaceutics*, 251(1–2), 33–47.
- Brès, G. A., & Colonius, T. (2008). Three-dimensional instabilities in compressible flow over open cavities. *Journal of Fluid Mechanics*, 599, 309–339. <https://doi.org/10.1017/S0022112007009925>
- Cattafesta, L. N., Song, Q., Williams, D. R., Rowley, C. W., & Alvi, F. S. (2008). Active control of flow-induced cavity oscillations. *Progress in Aerospace Sciences*, 44(7–8), 479–502. <https://doi.org/10.1016/j.paerosci.2008.07.002>
- Charwat, A. F. (1961). An Investigation of Separated Flows - Part I: The Pressure Field. *Journal of the Aerospace Sciences*, 28(6), 457–470.

- Chatellier, L., Laumonier, J., & Gervais, Y. (2004). Theoretical and experimental investigations of low Mach number turbulent cavity flows. *Experiments in Fluids*, 36(5), 728–740.
<https://doi.org/10.1007/s00348-003-0752-4>
- Cherdron, W., Durst, F., & Whitelaw, J. (1978). Asymmetric flows and instabilities in symmetric ducts with sudden expansions. *Journal of Fluid Mechanics*, 84, 13–31.
- Chisari, N. E., Artana, G., & Sciamarella, D. (2011). Vortex dipolar structures in a rigid model of the larynx at flow onset. *Experiments in Fluids*, 50(2), 397–406. <https://doi.org/10.1007/s00348-010-0941-x>
- Chow, A. H. L., Tong, H. H. Y., Chattopadhyay, P., & Shekunov, B. Y. (2007). Particle Engineering for Pulmonary Drug Delivery. *Pharmaceutical Research*, 24(3), 411–437. <https://doi.org/10.1007/s11095-006-9174-3>
- Cohen, J., Douma, W. R., ten Hacken, N. H. T., Vonk, J. M., Oudkerk, M., & Postma, D. S. (2008). Ciclesonide improves measures of small airway involvement in asthma. *European Respiratory Journal*, 31(6), 1213–1220. <https://doi.org/10.1183/09031936.00082407>
- Conway, J. (2012). Lung imaging — Two dimensional gamma scintigraphy, SPECT, CT and PET. *Advanced Drug Delivery Reviews*, 64(4), 357–368. <https://doi.org/10.1016/j.addr.2012.01.013>
- Cortelezzi, L., & Karagozian, A. R. (n.d.). *On the formation of the counter-rotating vortex pair in transverse jets*. 27.
- Coussement, A., Gicquel, O., & Degrez, G. (2012). Large eddy simulation of a pulsed jet in cross-flow. *Journal of Fluid Mechanics*, 695, 1–34. <https://doi.org/10.1017/jfm.2011.539>
- de Vicente, J., Basley, J., Meseguer-Garrido, F., Soria, J., & Theofilis, V. (2014). Three-dimensional instabilities over a rectangular open cavity: From linear stability analysis to experimentation. *Journal of Fluid Mechanics*, 748, 189–220. <https://doi.org/10.1017/jfm.2014.126>

- East, L. F. (1966). Aerodynamically induced resonance in rectangular cavities. *Journal of Sound and Vibration*, 3(3), 277–287.
- Ern, P., & Wesfreid, J. E. (1996). Pressure fluctuations in an unstable confined jet. *AIAA Journal*, 34(9), 1952–1954. <https://doi.org/10.2514/3.13334>
- Eroglu, A., & Breidenthal, R. E. (2001). Structure, Penetration, and Mixing of Pulsed Jets in Crossflow. *AIAA Journal*, 39(3), 417–423.
- Farkas, B., Paál, G., & Szabó, K. G. (2012). Descriptive analysis of a mode transition of the flow over an open cavity. *Physics of Fluids*, 24(2), 027102. <https://doi.org/10.1063/1.3687242>
- Fric, T., & Roshko, A. (1994). VORTICAL STRUCTURE IN THE WAKE OF A TRANSVERSE JET. *Journal Of Fluid Mechanics*, 279, 1–47.
- Gharib, M. (1987). Response of the cavity shear layer oscillations to external forcing. *AIAA Journal*, 25(1), 43–47.
- Gharib, M., & Roshko, A. (1987). The effect of flow oscillations on cavity drag. *Journal of Fluid Mechanics*, 177, 501–530. <https://doi.org/10.1017/S002211208700106X>
- Gloerfelt, X., & Lafon, P. (2008). Direct computation of the noise induced by a turbulent flow through a diaphragm in a duct at low Mach number. *Computers & Fluids*, 37(4), 388–401. <https://doi.org/10.1016/j.compfluid.2007.02.004>
- Gloerfelt, Xavier, Bogey, C., & Bailly, C. (2003). Numerical Evidence of Mode Switching in the Flow-Induced Oscillations by a Cavity. *International Journal of Aeroacoustics*, 2(2), 193–217. <https://doi.org/10.1260/147547203322775533>

- Guéniat, F., Pastur, L., & Lusseyran, F. (2014). Investigating mode competition and three-dimensional features from two-dimensional velocity fields in an open cavity flow by modal decompositions. *Physics of Fluids*, 26(8), 085101. <https://doi.org/10.1063/1.4891254>
- Haigermoser, C., Vesely, L., Novara, M., & Onorato, M. (2008). A time-resolved particle image velocimetry investigation of a cavity flow with a thick incoming turbulent boundary layer. *Physics of Fluids*, 20(10), 105101. <https://doi.org/10.1063/1.2990043>
- Hess. (2008). Aerosol Delivery Devices in the Treatment of Asthma. *RESPIRATORY CARE*, 53(6), 27.
- Heyder, J. (1982). Particle transport onto human airway surfaces. *European Journal of Respiratory Diseases. Supplement*, 119.
- Huang, R. F., & Hsu, C. M. (2012). Flow and mixing characteristics of an elevated pulsating transverse jet. *Physics of Fluids*, 24(1), 015104. <https://doi.org/10.1063/1.3678333>
- Illingworth, S. J., Morgans, A. S., & Rowley, C. W. (2012). Feedback control of cavity flow oscillations using simple linear models. *Journal of Fluid Mechanics*, 709, 223–248.
<https://doi.org/10.1017/jfm.2012.330>
- Johari, H. (2006). Scaling of Fully Pulsed Jets in Crossflow. *AIAA Journal*, 44(11), 2719–2725.
<https://doi.org/10.2514/1.18929>
- Kalter, R., Tummers, M. J., Kenjereš, S., Righolt, B. W., & Kleijn, C. R. (2013). Oscillations of the fluid flow and the free surface in a cavity with a submerged bifurcated nozzle. *International Journal of Heat and Fluid Flow*, 44, 365–374. <https://doi.org/10.1016/j.ijheatfluidflow.2013.07.007>
- Kegerise, M. A., Spina, E. F., Garg, S., & Cattafesta, L. N. (2004). Mode-switching and nonlinear effects in compressible flow over a cavity. *Physics of Fluids*, 16(3), 678–687. <https://doi.org/10.1063/1.1643736>

- Kelso, R. M., Lim, T. T., & Perry, A. E. (1996). An experimental study of round jets in cross-flow. *Journal of Fluid Mechanics*, 306, 111–144. <https://doi.org/10.1017/S0022112096001255>
- Kolšek, T., Jelić, N., & Duhovnik, J. (2007). Numerical study of flow asymmetry and self-sustained jet oscillations in geometrically symmetric cavities. *Applied Mathematical Modelling*, 31(10), 2355–2373. <https://doi.org/10.1016/j.apm.2006.10.010>
- Krishnamurty, K., United States, & National Advisory Committee for Aeronautics. (1955). *Acoustic radiation from two-dimensional rectangular cutouts in aerodynamic surfaces*. Washington, D.C.: National Advisory Committee for Aeronautics.
- Krothapalli, A., Lourenco, L., & Buchlin, J. M. (1990). Separated flow upstream of a jet in a crossflow. *AIAA Journal*, 28(3), 414–420.
- Kumar, M., & Vaidyanathan, A. (2018). On shock train interaction with cavity oscillations in a confined supersonic flow. *Experimental Thermal and Fluid Science*, 90, 260–274. <https://doi.org/10.1016/j.expthermflusci.2017.08.009>
- Labiris, N. R., & Dolovich, M. B. (2003). Pulmonary drug delivery. Part I: Physiological factors affecting therapeutic effectiveness of aerosolized medications: Physiological factors affecting the effectiveness of inhaled drugs. *British Journal of Clinical Pharmacology*, 56(6), 588–599. <https://doi.org/10.1046/j.1365-2125.2003.01892.x>
- Larchevêque, L., Sagaut, P., Mary, I., Labbé, O., & Comte, P. (2003). Large-eddy simulation of a compressible flow past a deep cavity. *Physics of Fluids*, 15(1), 193–210. <https://doi.org/10.1063/1.1522379>
- Laube, B. L., Janssens, H. M., de Jongh, F. H. C., Devadason, S. G., Dhand, R., Diot, P., ... Chrystyn, H. (2011). What the pulmonary specialist should know about the new inhalation therapies. *European Respiratory Journal*, 37(6), 1308–1417. <https://doi.org/10.1183/09031936.00166410>

Liu, W., Kang, Y., Zhang, M., Wang, X., & Li, D. (2017). Self-sustained oscillation and cavitation characteristics of a jet in a Helmholtz resonator. *International Journal of Heat and Fluid Flow*, 68, 158–172. <https://doi.org/10.1016/j.ijheatfluidflow.2017.10.004>

Lusseyran, F., Pastur, L., & Letellier, C. (2008). Dynamical analysis of an intermittency in an open cavity flow. *Physics of Fluids*, 20(11), 114101. <https://doi.org/10.1063/1.3005435>

M. Grace, S., Dewar, W. G., & E. Wroblewski, D. (2004). Experimental investigation of the flow characteristics within a shallow wall cavity for both laminar and turbulent upstream boundary layers. *Experiments in Fluids*, 36(5), 791–804. <https://doi.org/10.1007/s00348-003-0761-3>

Malone, J., Debiasi, M., Little, J., & Samimy, M. (2009). Analysis of the spectral relationships of cavity tones in subsonic resonant cavity flows. *Physics of Fluids*, 21(5), 055103. <https://doi.org/10.1063/1.3139270>

Margason, R. J. (1993). Computational and Experimental Assessment of Jets in Cross Flow. *AGARD*.

Martinez, M. A., Di Cicca, G. M., Iovieno, M., & Onorato, M. (2012). Control of Cavity Flow Oscillations by High Frequency Forcing. *Journal of Fluids Engineering*, 134(5), 051201. <https://doi.org/10.1115/1.4006468>

Mataoui, A., & Schiestel, R. (2009). Unsteady phenomena of an oscillating turbulent jet flow inside a cavity: Effect of aspect ratio. *Journal of Fluids and Structures*, 25(1), 60–79. <https://doi.org/10.1016/j.jfluidstructs.2008.03.010>

Mataoui, Amina, Schiestel, R., & Salem, A. (n.d.). *Flow Regimes of Interaction of a Turbulent Plane Jet into a Rectangular Cavity: Experimental Approach and Numerical Modelling*. 38.

Maurel, A., Ern, P., Zielinska, B. J. A., & Wesfreid, J. E. (1996). Experimental study of self-sustained oscillations in a confined jet. *Physical Review E*, 54(4), 3643–3651.

<https://doi.org/10.1103/PhysRevE.54.3643>

Murray, N., Sällström, E., & Ukeiley, L. (2009). Properties of subsonic open cavity flow fields. *Physics of Fluids*, 21(9), 095103. <https://doi.org/10.1063/1.3210772>

Nair, K. M., & Sarkar, S. (2016). Large Eddy Simulation of Self-Sustained Cavity Oscillation for Subsonic and Supersonic Flows. *Journal of Fluids Engineering*, 139(1), 011102.

<https://doi.org/10.1115/1.4034371>

Neary, M. D., & Stephanoff, K. D. (1987). Shear-layer-driven transition in a rectangular cavity. *Physics of Fluids*, 30(10), 2936. <https://doi.org/10.1063/1.866071>

Neubauer, J., Zhang, Z., Miraghaie, R., & Berry, D. A. (2007). Coherent structures of the near field flow in a self-oscillating physical model of the vocal folds. *The Journal of the Acoustical Society of America*, 121(2), 1102–1118. <https://doi.org/10.1121/1.2409488>

Newhouse, M. T., & Ruffin, R. E. (1978). Deposition and Fate of Aerosolized Drugs. *Chest*, 73(6), 936–943. https://doi.org/10.1378/chest.73.6_Supplement.936

Newman, S., Salmon, A., Nave, R., & Drollmann, A. (2006). High lung deposition of ^{99m}Tc-labeled ciclesonide administered via HFA-MDI to patients with asthma. *Respiratory Medicine*, 100(3), 375–384. <https://doi.org/10.1016/j.rmed.2005.09.027>

Özsoy, E., Rambaud, P., Stitou, A., & Riethmuller, M. L. (2005). Vortex characteristics in laminar cavity flow at very low Mach number. *Experiments in Fluids*, 38(2), 133–145. <https://doi.org/10.1007/s00348-004-0845-8>

Pope, S. B. (2000). *Turbulent Flows*. Cambridge: Cambridge University Press.

Powell, A. (1961). On the Edgetone. *The Journal of the Acoustical Society of America*, 33(4), 395–409.

<https://doi.org/10.1121/1.1908677>

Righolt, B. W., Kenjereš, S., Kalter, R., Tummers, M. J., & Kleijn, C. R. (2015). Dynamics of an oscillating turbulent jet in a confined cavity. *Physics of Fluids*, 27(9), 095107.

<https://doi.org/10.1063/1.4930926>

Rockwell, D., & Knisely, C. (1980a). Observations of the three-dimensional nature of unstable flow past a cavity. *Physics of Fluids*, 23(3), 425. <https://doi.org/10.1063/1.863009>

Rockwell, D., & Knisely, C. (1980b). Vortex-edge interaction: Mechanisms for generating low frequency components. *Physics of Fluids*, 23(2), 239. <https://doi.org/10.1063/1.862962>

Rockwell, D., & Naudascher, E. (1979). Self-Sustained Oscillations of Impinging Free Shear Layers.

Annual Review of Fluid Mechanics, 11(1), 67–94. <https://doi.org/10.1146/annurev.fl.11.010179.000435>

Rossiter, J. E. (1964). *Wind-tunnel experiments on the flow over rectangular cavities at subsonic and transonic speeds*. London: H.M.S.O.

Rowley, C. W., Colonius, T., & Basu, A. J. (2002). On self-sustained oscillations in two-dimensional compressible flow over rectangular cavities. *Journal of Fluid Mechanics*, 455, 315–346.

<https://doi.org/10.1017/S0022112001007534>

Rowley, C. W., & Williams, D. R. (2006). DYNAMICS AND CONTROL OF HIGH-REYNOLDS-NUMBER FLOW OVER OPEN CAVITIES. *Annual Review of Fluid Mechanics*, 38(1), 251–276.

<https://doi.org/10.1146/annurev.fluid.38.050304.092057>

Ruffin, R. E., Dolovich, M. B., Oldenburg, F. A., & Newhouse, M. T. (1981). The preferential deposition of inhaled isoproterenol and propranolol in asthmatic patients. *Chest*, 80(6 Suppl), 904–907.

- Ruffin, R. E., Dolovich, M. B., Wolff, R. K., & Newhouse, M. T. (1978). The effects of preferential deposition of histamine in the human airway. *The American Review of Respiratory Disease*, 117(3), 485–492.
- Ruiz, A. M., Lacaze, G., & Oefelein, J. C. (2015). Flow topologies and turbulence scales in a jet-in-cross-flow. *Physics of Fluids*, 27(4), 045101. <https://doi.org/10.1063/1.4915065>
- Sarohia, V. (1977). Experimental Investigation of Oscillations in Flows Over Shallow Cavities. *AIAA Journal*, 15(7), 984–991.
- Sau, R., & Mahesh, K. (2010). Optimization of pulsed jets in crossflow. *Journal of Fluid Mechanics*, 653, 365–390. <https://doi.org/10.1017/S0022112010000388>
- Schreck, E., & Schäfer, M. (2000). Numerical study of bifurcation in three-dimensional sudden channel expansions. *Computers & Fluids*, 29(5), 583–593. [https://doi.org/10.1016/S0045-7930\(99\)00014-6](https://doi.org/10.1016/S0045-7930(99)00014-6)
- Seena, A., & Sung, H. J. (2011). Dynamic mode decomposition of turbulent cavity flows for self-sustained oscillations. *International Journal of Heat and Fluid Flow*, 32(6), 1098–1110. <https://doi.org/10.1016/j.ijheatfluidflow.2011.09.008>
- Shankar, P. N., & Deshpande, M. D. (2000). Fluid Mechanics in the Driven Cavity. *Annual Review of Fluid Mechanics*, 32(1), 93–136. <https://doi.org/10.1146/annurev.fluid.32.1.93>
- Tam, C. (1976). The acoustic modes of a two-dimensional rectangular cavity. *Journal of Sound and Vibration*, 49, 353–364.
- Taherian, S., Rahai, H., Gomez, B., Waddington, T., and Bonifacio, J. (2015). "Tracheal Stenosis: A CFD Approach for Evaluation of Drug Delivery", IMECE2015-50799, Volume 3: Biomedical and Biotechnology Engineering. ASME 2015 International Mechanical Engineering Congress & Exposition, Houston, Texas, USA

Taherian, S., Rahai, H. R., Bonifacio, J., Gomez, B. Z., & Waddington, T. (2017). Particulate Deposition in a Patient With Tracheal Stenosis. *Journal of Engineering and Science in Medical Diagnostics and Therapy*, 1(1), 011005-011005–011010. <https://doi.org/10.1115/1.4038260>

Tuerke, F., Pastur, L. R., Sciamarella, D., Lusseyran, F., & Artana, G. (2017). Experimental study of double-cavity flow. *Experiments in Fluids*, 58(7), 76. <https://doi.org/10.1007/s00348-017-2360-8>

Ukeiley, L., & Murray, N. (2005). Velocity and surface pressure measurements in an open cavity. *Experiments in Fluids*, 38(5), 656–671. <https://doi.org/10.1007/s00348-005-0948-x>

Usmani, O. S., Biddiscombe, M. F., & Barnes, P. J. (2005). Regional Lung Deposition and Bronchodilator Response as a Function of β_2 -Agonist Particle Size. *American Journal of Respiratory and Critical Care Medicine*, 172(12), 1497–1504. <https://doi.org/10.1164/rccm.200410-1414OC>

van den Berge, M., ten Hacken, N. H. T., van der Wiel, E., & Postma, D. S. (2013). Treatment of the bronchial tree from beginning to end: Targeting small airway inflammation in asthma. *Allergy*, 68(1), 16–26. <https://doi.org/10.1111/all.12062>

Vermeulen, P. J., Chin, C.-F., & Yu, W. K. (1990). Mixing of an acoustically pulsed air jet with a confined crossflow. *Journal of Propulsion and Power*, 6(6), 777–783.

Wang, Y., Tan, L., Wang, B., Cao, S., & Zhu, B. (2015). Numerical Investigation on Frequency Jump of Flow Over a Cavity Using Large Eddy Simulation. *Journal of Fluids Engineering*, 137(8), 081203. <https://doi.org/10.1115/1.4030002>

Yokoyama, H., & Kato, C. (2009). Fluid-acoustic interactions in self-sustained oscillations in turbulent cavity flows. I. Fluid-dynamic oscillations. *Physics of Fluids*, 21(10), 105103. <https://doi.org/10.1063/1.3253326>